PERFORMANCE OF A CENTRIFUGALLY CONTROLLED VARIABLE GEOMETRY VERTICAL AXIS WIND TURBINE

by

Rishi Raj Pandey

DEPARTMENT OF AEROSPACE ENGINEERING

INDIAN INSTITUTE OF TECHNOLOGY KANPUR

APRIL, 1996

PERFORMANCE OF A CENTRIFUGALLY CONTROLLED VARIABLE GEOMETRY VERTICAL AXIS WIND TURBINE

A Thesis Submitted
In Partial Fulfilment of the Requirements
for the Degree of

MASTER OF TECHNOLOGY

By

RISHI RAJ PANDEY

to the

DEPARTMENT OF AEROSPACE ENGINEERING

INDIAN INSTITUTE OF TECHNOLOGY KANPUR

APRIL, 1996

AE-1996-M-PAN-PER

Dedicated

To

My Father

SRI RAJ KUMAR PANDEY

CERTIFICATE

This is to certify that the work entitled *Performance of a Centrifugally Controlled Variable Geometry Vertical Axis Wind Turbine* is the record of the work carried out by Rishi Raj Pandey under my supervision and has not been submitted elsewhere for the award of a Degree.

April 3 ,1996

(Dr. Kunal Ghosh)
Professor
Department of Aerospace Engineering
INDIAN INSTITUTE OF TECHNOLOGY
KANPUR (INDIA).

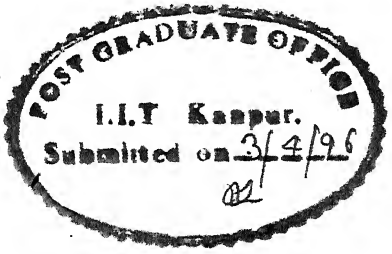

ACKNOWLEDGEMENTS

I wish to express my gratitude to my thesis supervisor Dr. Kunal Ghosh for his guidance throughout my M.Tech. programme and motivation towards Wind Energy research. I am also grateful to all those professors who have taught me at I.I.T. Kanpur.

I am thankful to my friends specially Sanjay Kumar, Manoranjan Sinha and Rajeev Gupta for their lively and memorable company during my stay at I.I.T. Kanpur. I am also thankful to Rakesh Bassan for his help in initial stages of thesis typing.

Finally, I would be failing in my duty if I do not express my gratitude to my respected father, Sri Raj Kumar Pandey, for his invaluable guidance and sacrifice throughout my career. He has been a constant source of inspiration for me. I am highly indebted to him.

Rishi Raj Pandey

I.I.T. KANPUR.

NOMENCLATURE

A	Unreefed swept area of rotor
A'	Swept area of rotor when it is reefed
A_∞	Stream tube area far away from the disc
A_w	Stream tube area at the wake
a	Axial interference parameter at the disc
b	Axial interference parameter at the wake
	(Quarter blade length)
C	Chord length
C_d	Section drag coefficient
C_l	Section lift coefficient
C_n	Normal force coefficient acting normal to the chord
C_t	Tangential force coefficient acting along the chord
C_P	Power coefficient of wind turbine
C_P'	Power coefficient of wind turbine based on V
C_T	Thrust coefficient of wind turbine
C_T'	Thrust coefficient of wind turbine based on V
C_Q	Torque coefficient
dD	Elemental drag
dL	Elemental lift
dQ	Elemental torque
dT	Elemental thrust
E_g	Generator efficiency
E_{trans}	Drive train efficiency
G	Ratio of quarter blade length to strut length
k	Theoretical $(C_P)_{max} = 16/27$
k_1	$= (A/R^2)$
L	Strut length

N	Number of blades
P_∞	Free stream static pressure
P^+	Pressure acting in front of the disc
P^-	Pressure acting on the back side of the disc
P	Mean power produced by the turbine
P_{hb}	Mean power produced by the half blade
Q	Mean torque on the rotor
R	Unreefed radius of the turbine
R'	Radius of the turbine when it is reefed
T	Mean thrust acting on the turbine
U	Relative velocity of the blade in the plane of the blade section
U_R	Relative velocity of the blade in the horizontal plane
V_∞	Free stream wind speed
V	Wind speed at the disc
α	Angle of attack
β	Arrowhead angle
ϕ	Azimuthal angle
Γ	Reef angle
ρ_∞	Free stream air density
Ω	Angular velocity of the turbine
θ	Strut angle
θ_o	Strut angle for $\Gamma = 0^\circ$
σ	Solidity = NC/R
λ	Tip speed ratio based on V_∞ ($= \frac{\Omega R}{V_\infty}$)
λ'	Tip speed ratio based on V ($= \frac{\Omega R}{V}$)
ω_o	Rated angular velocity
L_b	Half blade length

C_b Blade chord length

M_b Mass of the half blade

cg_b C.G. Location of the half blade

W_{ep} Width of the end plate

t_{ep} Thickness of the end plate

L_{ep} Length of the end plate

M_{ep} Mass of the end plate

W_{sl} Width of the sleeve

t_{sl} Thickness of the sleeve

h_{sl} Height of bearing sleeve or pad

bear_s Space between the bearings

X_h Location of the strut hinge

X_x Location of the near end of X - arm (Unreefed)

M_x Mass of the X - arm

ϕ_o Azimuthal angle at t = 0

V_j Velocity at the disc after jump

α_o Angle of attack at t = 0

α_j Angle of attack after jump in velocity at the disc

Q_o Aerodynamic torque at t = 0

Q_j Aerodynamic torque after jump

Q_g Generator torque

Q_{hb} Aerodynamic torque produced by the half blade

V_x Radial velocity of the cross-arm

ω Angular velocity

L_s Strut length

F_{cx} Net outward force in the cross-arm

F_2 Force in the upper hinge (Fig.6.7)

F_2' Force in the lower hinge (Fig.6.7)

r C.G. location of the cross-arm (unreefed case) (Fig.6.6)

r' C.G. location of the cross-arm (reefed case) (Fig.6.7)

h_z Height of the upper hinge from sleeve

θ_s Strut angle

F_s Strut force

LIST OF FIGURES

ABSTRACT

A Variable Geometry Vertical Axis Wind Turbine with a novel control system proposed by Dr. Ghosh in 1990, called as centrifugal reef control system, has been chosen for the present study for having certain advantages over other types of wind turbines. The aerodynamic design parameters such as radius of the turbine, blade length and chord have been chosen so as to generate approximately 10 kW of power at a wind speed of 10 m/s. Templin's procedure, which avoids iteration,has been followed in the context of Rankine Froude Momentum theory to relate the induced velocity at actuator disc to free stream velocity. To solve equations numerically, Newton - Cotes technique has been used and a FORTRAN code has been developed for this purpose. For simplicity, the induced velocity is assumed to be uniform over the entire swept area of rotor. Blade element analysis has been used to derive the aerodynamic performance characteristics (i.e. power, thrust and torque coefficients) of the wind turbine. The aerodynamic characteristics have also been studied for reefed configurations. The effect of solidity on power coefficient has been presented. The power coefficient for different reefed conditions has been compared with other available theories and experiments. Aerodynamic forces acting on the blades have been estimated for the unreefed condition when they are at their maxima. A summary of the work done on VGVAWT at IIT Kanpur has been presented in the end.

INTRODUCTION

Winds result from the fact that the earth's equatorial regions receive more solar energy than the polar regions,and this sets up large scale convection currents in the atmosphere. Meteorologists estimate that about 1% of the incoming solar radiation is converted into wind energy. The solar energy received by the earth in just 10 days has an energy content nearly equal to the world's entire fossil fuel reserves (coal, oil & gas). This means that the wind resource is extremely large. As the fossil fuels are exhaustible, sufficient power will not be produced using these conventional sources of energy in the near future. Consequently, we have to go in for alternative sources of energy which are renewable like Solar, Wind and Biomass energy etc.

It has been realized by now that wind is a clean (non - polluting) and renewable source of energy from which electrical and mechanical power may be generated. Right from the beginning of civilization, people used to harness the wind energy for useful purposes like pumping water, grinding grains, sailing ships etc. Over the last 2000 years or so, different types of wind machines have been invented. Wind energy research and development work are being done in U.K., USA, China, Japan, India and many other countries.

In India,the Government has also realized the potential of renewable resources of energy and it has taken various steps in this regard. In 1987, Government of India set up Indian Renewable Energy Development Agency (IREDA) to finance commercially viable projects.

Rapid progress is being made in the development and demonstration of wind energy. Till March 1995, a capacity of about

275 MW of wind energy generation has been established; including private sector projects [26]. The Govt. has extended a package of incentives for wind power generation. This includes loans from IREDA at concessional interest rates, tax holiday for 5 years, exemption from excise duty and exemption or reduced rate for custom duty on imports of wind turbines. IREDA has initiated the '' India Renewable Resources Development Project '' consisting of three projects having ' Wind - farm Development ' as one of the projects. Till March 1995, IREDA had sanctioned nearly 400 renewable energy projects for about Rs. 360 crores for manufacture and installation of new and renewable sources of energy systems and devices.

Department of Non-conventional Energy Sources (DNES) has started its programmes at various places all over India like Tuticorin (Tamilnadu), Mandvi and Okha (Gujarat) and Puri (Orissa) etc. in cooperation with various State Electricity Boards in 1986 [12]. The Govt. of India has announced various policy measures to encourage direct foreign investments and collaborations.

A Variable Geometry Vertical Axis Wind Turbine (VGVAWT) has been chosen for the present analysis for having its own distinguished advantages over Horizontal Axis Wind Turbine (HAWT) from design point of view though it has a few disadvantages also. A critical and comparative assessment of both VAWT and HAWT has been made and VGVAWT with centrifugal reef control (proposed by Dr. Ghosh) has been chosen. Wind Energy survey in India identifies many wind rich areas all over the country. The average annual mean wind speed is found to vary from 6 m/s to 10 m/s in places like Tuticorin,Okha etc. [12].

CHAPTER - 1

Literature survey :

In 1930 Darrieus first developed a VAWT which utilizes the lift force. Before his period, people used to try with lift devices and drag devices separately. Darrieus used a blade with Troposkien shape, which can be explained as following :

When a rope is rotated about a vertical axis at a particular r.p.m. , it takes a special shape called as 'Troposkien shape'. The centrifugal force acting at each point on such curve will be balanced by the tensile force of the rope. Hence, it is advantageous to use blades of this shape. But making Troposkien shape without bending a straight blade (i.e. without introducing pre - stresses) is very difficult.

The power produced by the turbine depends on the wind speed. Most of the wind turbines are located in coastal areas since they have high wind power potential throughout the year. The coastal areas are often prone to cyclones and hence a wind turbine with the straight blades with fixed geometry may experience severe loadings. Musgrove [1976] suggested a variable geometry vertical axis wind turbine and a 25 m. diameter, 160 kW prototype machine was installed in Carmarthen Bay. Reefing was achieved hydraulically through a computer controlled system. The experience and the data gathered on this machine was utilized in constructing a 17m diameter 100 kW variable geometry VAWT on the Isles of Scilly (Mays et al, 1987). In late 1987, there was a failure in the reefing control mechanism which led to an overspeed situation causing damage to the rotor (Mays 1989, Lindley 1988/89). Data gathered from the 25m wind turbine at Carmarthen Bay has shown that a stall regulated fixed geometry rotor gives less severe

loading than had been anticipated (Mays 1989). Later the wind turbine was replaced by a stall regulated fixed geometry rotor where beyond certain wind speed, the rotor is held at a constant r.p.m. by the grid causing the blades to stall and thus the wind turbine is controlled.

The variable geometry concept is a novel idea to get a constant rated power and maintain a constant r.p.m. The angular speed should be maintained constant in the case of electricity generation to achieve a steady frequency, for ex. 50 Hz, in the case of electric power generation for the grid.

On comparing VAWT & HAWT, we see that both have advantages as well as disadvantages. The VAWT is able to extract energy from the wind independent of the wind direction, i.e., VAWTs are omnidirectional so that one can avoid the cost and complexity of a yaw orientation sub - system. Due to the fact that the rotor has a fixed pitch and low solidity, VAWT is not self starting. One of the attractions of the vertical axis configuration is that it eliminates the cyclically varying stresses which the blades of HAWT experience, due to their weight, as they rotate. These cyclically varying gravity stresses become progressively more dominant as the overall turbine size increases, and imposes a theoretical limit on the size of the horizontal axis rotor. Although VAWT blades experience cyclically varying aerodynamic loads, the resulting stresses remain substantially constant as the turbine size is increased.

The novel idea of reefing (i.e. deflecting the blade w.r.t. a vertical axis to resemble an arrowhead) was achieved (Anderson et. al.,1987) by a hydraulic system which senses the over speed of the wind or wind turbine and allows the blade to reef. The

conditions and rotor was replaced by a fixed geometry stall regulated one. Dr. K. Ghosh (1990) suggested a novel method of reef control viz. centrifugal reef control technique. He argues that since the radial component of the aerodynamic forces acting on a blade is outward during one half of the rotation and inward during the other half, its contribution in assisting the centrifugal forces on an average can be ignored. He showed that with a realistic mass distribution among various members (i.e. blade, cross - arm etc.) , the centrifugal force varies fairly linearly with distance of the C.G. from the axis of rotation. This force, therefore, can be balanced against a linear spring [Fig.3.2] . To limit the to and fro motion due to aerodynamic force changing direction, dampers are necessary [Fig.3.2] . He developed a method to find the centrifugal force and relation between the reef angle and the change of radius with reef angles. Hence it is possible to assess the stiffness of the spring which is capable of withstanding the centrifugal force for reefing angle from 0 to 90 degrees from his analysis. His analysis also shows that the centrifugal reef control is cheap and quite reliable. Moreover, the control system is simple to design.

Design of such wind turbine involves thrust and power calculations based on geometry for various wind speeds and rpms. Templin [1974] deviced a methodology to find out the average power and thrust coefficients which avoids an iterative procedure. The above procedure was adopted by Shankar [1976] and he calculated the performance of a Darrieus wind turbine assuming both uniform induced velocity and non - uniform induced velocity approaches.

Rankine Froude momentum theory further developed by Glauert [1963] , wherein the wind turbine is assumed

and interference factor. This theory is generally used by any wind turbine designer for preliminary design calculations. But one should realize that this theory will not be adequate to analyze what exactly happens to the flow that passes through a vertical axis wind turbine. The actuator cylinder flow theory discussed by Freris [1990], predicts the flow velocities just upstream and downstream of the turbine.

In 1992, Selvaraj, an M.Tech. student in Aerospace Engg. Department at I.I.T. Kanpur worked on VGVAWT under the guidance of Dr. Ghosh . His formulation of the problem and computer program have been rechecked now (1996). There were some errors in his computer program and those have been removed now. His graphs have been rechecked and some modifications in his formulation have been made as suggested by Dr. Ghosh. The computer program has been modified accordingly.

2.1 Aerodynamic Modelling :

2.1.1 Rankine Froude Momentum Theory :

This theory is based upon following assumptions :

1) The wind is steady and homogeneous

2) The flow is inviscid and incompressible

3) The flow is one dimensional and has no rotational velocity

4) The wind turbine is considered as a simple actuator disc

5) The wind has constant velocity over the disc and over the cross-section of the ultimate wake.

The flow past a wind turbine is as shown in Fig. 2.1 . The free stream wind, V_∞ is slowed down to V at the disc and it is further decelerated to u. During this process, wind machine extracts energy from the wind. The fluid which has passed or will pass through the wind turbine disc forms a cylindrical duct whose cross-sectional area increases from A_∞ far in front of the disc to A at the wind turbine disc and finally to A_w at the ultimate wake (Fig.2.1).

To proceed further with the development of the theory, it is necessary to consider the form of the momentum equation as applied to individual annular elements of the wind turbine,i.e., to the fluid which passes through the turbine between the radii r and (r+dr).

The system of forces acting on the control volume of fluid bounded at the ends by the two sections, A_∞ and A_w far upstream and downstream the turbine comprises of the thrust T, the pressure

force $P_\infty(A_w - A_\infty)$ over the ends of the control volume and an axial force X due to the pressure on the lateral boundary of control volume. Then the momentum equation for the control volume of fluid can now be expressed as ---

$$T - X + P_\infty(A_w - A_\infty) = \int \rho_\infty u(V_\infty - u)\, dA_w \qquad \ldots.(2.1)$$

where the integral extends over the cross-section of the wake and the velocity u may have different values for different annular elements.

It has been shown in Ref.[10] that the axial pressure force X on the lateral boundary of the control volume of fluid is equal to the pressure force $P_\infty(A_w - A_\infty)$ acting at both ends. Therefore the Eqn.(2.1) becomes ----

$$T = \int \rho_\infty u\,(V_\infty - u)\, dA_w \qquad \ldots.(2.2)$$

Due to the assumption no.(5), the above eqn. may be written in a very simple form as ----

$$T = \rho_\infty A_w u\,(V_\infty - u) \qquad \ldots..(2.3)$$

By continuity, we have -

$$\dot{m} = \rho_\infty A_\infty V_\infty = \rho_\infty A V = \rho_\infty A_w u \qquad \ldots(2.4)$$

Introducing Eqn.(2.4) into Eqn.(2.3), we get -

$$T = \dot{m}\,(V_\infty - u) = \rho_\infty A V\,(V_\infty - u) \qquad \ldots.(2.5)$$

Applying Bernoulli's equation between the sections 0 and 3, and 2 and 1 (Fig.2.1) , we have -

$$P_\infty + (1/2)\,\rho_\infty V_\infty^2 = P^+ + (1/2)\,\rho_\infty V^2 \qquad \ldots..(2.6\ a)$$

$$P^- + (1/2)\,\rho_\infty V^2 = P_\infty + (1/2)\,\rho_\infty u^2 \qquad \ldots..(2.6\ b)$$

Also the thrust acting on the air must be equal to the thrust acting on the wind turbine which is nothing but the area times the pressure difference acting on either side of the turbine.

i.e.,

$$T = A\,(P^+ - P^-) \qquad \ldots.(2.7)$$

$$P^+ - P^- = (1/2)\,\rho_\infty (V_\infty^2 - u^2) \qquad \ldots(2.8)$$

Therefore Eqn.(2.7) becomes

$$T = (1/2)\,\rho_\infty A\,(V_\infty^2 - u^2) \qquad \ldots.(2.9)$$

Comparing Eqns.(2.3) and (2.8), it is seen that

$$V = (V_\infty + u)/2 \qquad \ldots\ (2.10)$$

Thus the velocity at the disc is the average of the upstream and downstream velocities.

Defining axial interference parameters, a and b as the fractional decreases in wind velocity at the rotor plane and wake, represented by

$$V = V_\infty\,(1 - a) \qquad \ldots.(2.11)$$

and $$u = V_\infty\,(1 - b) \qquad \ldots.(2.12)$$

respectively. From Eqn.(2.10), it is obvious that $b = 2a$. From Eqns.(2.11) and (2.12), we can infer that when $a = 0$, no power is absorbed, whereas for $a = 0.5$ (i.e. $b = 1$), the wind has zero velocity at the wake. When $a = 1$, the flow has zero velocity right at the disc and hence the streamlines break away from the turbine. Because of this flow behaviour at the disc, the stream tube theory i.e. the Rankine Froude's momentum theory can not be used in this condition of operation.

The energy removed by the rotor per unit time is

$$P = (1/2)\rho_\infty V_\infty^2\, A\, V - (1/2)\rho_\infty u^2 A\, V$$

i.e.,

$$P = (1/2)\,\rho_\infty A\, V\,(V_\infty + u)(V_\infty - u) \qquad \ldots(2.13)$$

Substituting for V from Eqn.(2.11) and u from Eqn.(2.12), the above Eqn. becomes

$$P = (1/2)\,\rho_\infty A\, V_\infty^3\,(4\,a)(1 - a)^2 \qquad \ldots..(2.14)$$

Defining the power coefficient C_P as

$$C_P = \frac{P}{(1/2)\,\rho_\infty A\, V_\infty^3} \qquad \ldots.\ (2.15)$$

Then C_P , while substituting for P from Eqn.(2.14) becomes

$$C_P = 4a(1 - a)^2 \qquad .....(2.16)$$

Similarly, we can define the thrust coefficient C_T as

$$C_T = \frac{T}{(1/2)\ \rho_\infty A\ V_\infty^2} \qquad .....(2.17)$$

Introducing the Eqns.(2.11) and (2.12) in (2.9) to get T , and then from Eqn.(2.17) C_T becomes ---

$$C_T = 4a(1 - a) \qquad .....(2.18)$$

By maximizing C_P , it can be easily shown that the max. power can be extracted when a = 1/3. The corresponding value of C_P is,

$$(C_P)_{max} = 16/27 \qquad ....(2.19)$$

The wind velocities at the max. power condition are

$$V = 2/3\ V_\infty \qquad .....(2.20\ a)$$

$$u = 1/3\ V_\infty \qquad .....(2.20\ b)$$

Eqn.(2.19) is called Betz efficiency and this does not represent the max. efficiency of the machine since the mass flow rate through the disc is not AV_∞ but AV. Hence, the efficiency i.e. power output divided by power available is given by --

$$\frac{P}{(1/2)\ \rho_\infty A\ V\ V_\infty^2} = 4a(1 - a) \qquad ....(2.21)$$

The max. efficiency is 100% at a = 1/2 which yields a power coefficient (C_P) of 0.5. Thus the efficiency at the max. power coefficient(i.e. C_P = 16/27) is 88.8% .(Putting a = 1/3 in Eqn.(2.21)).

The flow pattern and the flow properties of wind along the horizontal axis of a wind turbine are shown in Fig. 2.2 .

2.1.2 Definition Of Power and Thrust Coefficients :

The conventional definition for thrust and power

coefficients are, as given before,

$$C_T = \frac{T}{(1/2)\ \rho_\infty A\ V_\infty^2}$$

$$C_P = \frac{P}{(1/2)\ \rho_\infty A\ V_\infty^3}$$

Shankar [1976] has introduced two new coefficients C_P' and C_T' based on local wind speed at the rotor disc. He redefines the power coefficients C_P and C_P' with a factor k = 16/27 in the denominator in order to normalize w.r.t. the theoretical max. But , we shall not use his definition but stick to convention.

Therefore, we define

$$C_P' = \frac{P}{(1/2)\ \rho_\infty A\ V^3}$$

His definition of C_T and C_T' are according to convention, therefore

$$C_T' = \frac{T}{(1/2)\ \rho_\infty A\ V^2} \qquad \ldots.(2.22)$$

Making use of Eqns.(2.17) and (2.18),

$$C_T' = C_T\ (V_\infty /V)^2$$

$$= 4\ (V_\infty /V - 1) \quad \text{(using Eqn.(2.11))}$$

Hence,

$$(V/V_\infty) = \frac{1}{1 + C_T'/4} \qquad (2.23)$$

CHAPTER - 3

3.1 Parameter identification :

3.1.1 Rotor Area required :

Any Wind Energy Conversion System (WECS) will have the followi subsystems :

Rotor, power transmission system and electric generator.

Each of these subsystems has its own efficiency. Therefore, the total power extracted by a WECS may be written as ---

$$P = C_p \, E_{trans} \, E_g \, (1 / 2) \, \rho_\infty A \, V_\infty^3 \qquad \ldots\ldots\ldots (3.1)$$

where,

C_p = wind rotor power coefficient

E_{trans} = transmission system efficiency

E_g = generator efficiency

A = swept area required

V_∞ = wind speed

ρ_∞ = air density at the rotor hub.

The existing wind turbines at Tuticorin are at about 20 m. elevation from the ground and hence the density at 20 m. altitude is not very different from sea - level density of air, ρ_∞ = 1.225 kg/m^3. A modern and well designed wind turbine will have C_p around 0.45 . Also, we can choose the values of E_g and E_{trans} as 0.85 and 0.75 respectively for practical purposes. From wind energy survey conducted in India, especially in Tuticorin we conclude that the optimum rated wind speed is approximately 10 m/s [20]. So the design rated wind speed could be taken as 10 m/s.

After choosing the above parameters, the rotor area required for

10 kW wind turbine can be found as --

$$A = \frac{P}{(1/2)\ \rho_\infty V_\infty^3\ C_p E_{trans}\ E_g}$$

$$\simeq 57\ m^2 \quad (\text{after calculation})$$

Hence, $A \simeq 57\ m^2$

3.1.2 Rotor radius, Blade length and chord :

Sir Robert Mcalpine & Sons Ltd.[1986] designed a 25 m., 130 kW VGVAWT for Department of Energy, U.K. They arrived at some optimum ratio between the radius of the rotor and blade length after iterative calculations which are attributed to the structural consideration of the wind turbine. So it is reasonable to choose some proportions for the radius and blade length of the 10 kW VGVAWT as they did. Accordingly, following values of the rotor radius and blade length have been chosen ---

Rotor radius, R = 4.5 m

Blade length = 6.5 m

In the same manner the chord is also chosen as --

Chord, C = 0.45 m

Hence, the rotor area $A = 9 \times 6.5\ m^2$ (refer Fig.3.1)

$= 58.5\ m^2$

3.2 General Arrangement of the VGVAWT :

The general arrangement of the VGVAWT is as shown in Fig.3.1. It is proposed to have the no. of blades, N = 2. The horizontal telescopic cross-arm supports the two half blades on one side. On the other side the cross-arm is connected via a spring to a point on the rotor axis. Each half blade is connected via a control

strut to the sleeve which houses the telescopic cross-arm (Fig 3.2) . The whole arrangement of rotor is supported on a cantilever tower (Fig. 3.1) .

3.3 Airfoil Selection :

The VAWT extracts power both from the wind upstream and downstream of the tower, hence the airfoil encounters not only positive angles of attack but negative angles of attack also. The performance of the rotor depends on the (L/D) of the airfoil since it uses the lift force to generate power. The cambered airfoil has poor (L/D) for negative angles of attack for a given conditions. Therefore we select a symmetrical airfoil which has a reasonably good (L/D) for both positive and negative angles of attack.

NACA 0012 airfoil has been chosen for the computation. The blades are fixed at zero pitch to the circular path it traces.

4.1 Formulation of the problem :

The behaviour of a VGVAWT shown in Fig.(4.1) can be qualitatively understood by studying the figures(4.2) & (4.3). These figures show elemental section of a blade at various azimuthal position, ϕ, for a given wind speed V_∞ and at a particular angular speed Ω. When the local azimuthal speed $r\Omega$ is large compared to the local wind speed V, the blade element is unstalled for all ϕ as the effective angle of attack α is small. In this condition, the lift dL contributes positively to the torque while elemental drag dD detracts from it. On the other hand when $r\Omega < V$, the effective angle of attack can vary from 0° to $\pm 180^\circ$, ie, the blade may be stalled and or in reversed flow over part of its trajectory.

4.1.1 Expression for Radius and Area in terms of Arrowhead angle β

The expressions for R & A are found in terms of the reef angle Γ (see Figs.(3.2), and (4.4)) as follows; Since radius is changing with Γ, it is denoted as R' (Fig. 4.4) to differentiate from R which refers to the radius of the rotor (Fig. 3.1) corresponding to $\Gamma = 0$ and likewise swept area is denoted as A', where A represents the swept area when the turbine is unreefed. As the strut links the blade (at C.G.) and the cross arm it is necessary to find its length for $\Gamma = 0$. In order to counterbalance as far as possible the centrifugal force acting on the rotor blade, the strut should be connected as near to axis of rotation as possible so that it makes a low angle. Since the tower

has diameter of the order of R/10 it is not practically possible to fix the strut exactly at the axis. Therefore, the strut is fixed at a distance R/10 from the axis of rotation. From the Fig.(4.4), the strut length, L for $\Gamma = 0$ (or $\beta = 90$) can be calculated as

$$L = \sqrt{(\frac{9}{10} R)^2 + b^2}$$

where b is the quarter blade length.

Let $G = \frac{b}{L}$

For b = 1.62 m and R = 4.5 m , L becomes 4.36 m and hence G works out to be 0.37. Refering to Fig.(4.4), one can write an expression for R' as

$$R' = \frac{R}{10} + L \cos\theta + b \cos\beta$$

where θ is called strut angle and β arrowhead angle. Note $\Gamma = 90^\circ - \beta$. It is convenient to work in terms of the arrowhead angle.

Also, $L \sin\theta = b \sin\beta$

i.e.

$$\cos\theta = \sqrt{1 - G^2 \sin^2\beta}$$

Therefore,

$$R' = \frac{R}{10} + L \sqrt{1 - G^2 \sin^2\beta} + b \cos\beta$$

From Fig.(4.6), we have for $\beta = 90^\circ$,

$$\frac{0.9 R}{L} = \cos\theta_o \qquad (4.1a)$$

$$\frac{b}{0.9\ R} = \tan\theta_o \text{ and} \qquad (4.1b)$$

$$\frac{b}{L} = G = \sin\theta_o \qquad (4.1c)$$

where, $\theta = \theta_o$ when $\beta = 90^\circ$

Hence, R′ can be expressed as

$$R' = \frac{R}{10} + \frac{0.9\ R}{\cos\ \theta_o} \sqrt{1 - \sin^2\theta_o \sin^2\beta} + 0.9\ R \tan\ \theta_o \cos\ \beta$$

i.e. $R' = R\ f_1$ (4.2)

where, $f_1 = \frac{1}{10} + 0.9 \sqrt{\sec^2\theta_o - \tan^2\theta_o \sin^2\beta} + 0.9 \tan\ \theta_o \cos\ \beta$

(4.3)

The swept area A′ can be found refering to Fig.(4.5) as

$$A' = (2\ R' \times 4\ b \cos\ \Gamma) - (8\ b^2 \cos\ \Gamma \sin\ \Gamma)$$

i.e. $A' = 8R'b \sin\beta - 8b^2 \cos\beta \sin\beta$

i.e. $A' = 8b \sin\beta\ (R' - b\cos\beta)$

Using Eqns.(4.1b) and (4.2), the above Eqn. becomes

$$A' = 8 \times 0.9R \tan\theta_o \sin\beta (R\ f_1 - 0.9R \tan\theta_o \cos\beta\ )$$

i.e. $A' = 8R^2 \times 0.9 \tan\theta_o \sin\beta\ (f_1 - 0.9 \tan\theta_o \cos\beta\ )$ (4.4)

Also swept area corresponding to unreefed conditions is given by

$$A = 8Rb$$

Substituting for b from Eqn.(4.1b), we get

$$A = 8R^2 \times 0.9 \tan\theta_o \qquad (4.5)$$

After introducing Eqn. (4.5) into Eqn. (4.4), we get

$$A' = A \sin\beta \, [f_1 - 0.9 \tan\theta_o \cos\beta]$$

i.e. $$A' = A f_2 \qquad (4.6)$$

where $$f_2 = \sin\beta \, [f_1 - 0.9 \tan\theta_o \cos\beta] \qquad (4.7)$$

4.1.2 The Radius of a Blade Element:

Let us consider an element ds at (r,- z) in the Fig.(4.4). The analysis is first carried out for this lower half blade and then it can be generalised for the whole wind turbine. The radius of a blade element, can be written as

$$r = R' + z \cot\beta$$

where z varies from - 2b $\sin\beta$ to 0.

By non - dimensionalising with the unreefed radius R, we get

$$\bar{r} = \bar{R}' + \bar{z} \cot \beta \qquad (4.8)$$

where $\bar{r} = \frac{r}{R}$, $\bar{R}' = \frac{R'}{R}$ & $\bar{z} = \frac{z}{R}$

4.1.3 Blade Element Analysis:

We define the following unit vectors.

$\bar{e}_x$ = unit vector along x-direction

$\bar{e}_y$ = unit vector along y-direction

$\bar{e}_z$ = unit vector along z-direction

$\bar{e}_c$ = unit vector along the chord of the airfoil blade section

$\bar{e}_n$ = unit vector along the normal to the blade axis and perpendicular to the blade chord.

The co-ordinate system is shown in Fig.(4.6). It is obvious that $\bar{e}_n$ makes an angle β with the vertical.

$$\bar{e}_n = - \cos\beta\ \bar{e}_z + \sin\beta\ (\cos\phi\ \bar{e}_x + \sin\phi\ \bar{e}_y) \tag{4.9}$$

$$\bar{e}_c = - \sin\phi\ \bar{e}_x + \cos\phi\ \bar{e}_y \tag{4.10}$$

and for the elemental length ds located at a radius r from z-axis

$$ds = \frac{dz}{\sin\beta} \tag{4.11}$$

also

$$\sin\beta = \frac{1}{\sqrt{1 + (dr/dz)^2}}$$

Under unreefed conditions, the relative velocity at the blade section, U_R is given by

$$\bar{U}_R = - V\ \bar{e}_y + r\Omega\ (\sin\phi\ \bar{e}_x - \cos\phi\ \bar{e}_y) \tag{4.12}$$

However, the wind speed contributing to the lift and drag is given by the component of U_R in the plane of the blade section. This component U is given by

$$U^2 = (\bar{U}_R \cdot \bar{e}_n)^2 + (\bar{U}_R \cdot \bar{e}_c)^2$$

ie, $U^2 = (r\Omega + V\cos\phi)^2 + (V\sin\phi \ \sin\beta)^2$ (4.13)

The effective angle of attack α at the blade section is given by

$$\tan\alpha = \frac{\bar{U}_R \cdot \bar{e}_n}{\bar{U}_R \cdot \bar{e}_c} = \frac{V\sin\beta\sin\phi}{r\Omega + V\cos\phi} \quad (4.14)$$

4.1.4 Equation of Mean Power and Mean Thrust:

If the blade is of chord C with sectional lift and drag coefficients C_l and C_d, then the elemental lift and drag are given by

$$dL = (1/2)\,\rho_\infty U^2\, C\, C_l\, ds \quad (4.15)$$

$$dD = (1/2)\,\rho_\infty U^2\, C\, C_d\, ds \quad (4.16)$$

At the azimuthal position ϕ, the quasi-steay torque dQ and thrust dT due to element ds are given by

$$dQ = r\{dL\sin\alpha - dD\cos\alpha\}$$

$$dT = -\cos\phi\{dL\sin\alpha - dD\cos\alpha\} + \sin\beta\sin\phi\{dL\cos\alpha + dD\sin\alpha\}$$

respectively.

By Eqns. (4.15) and (4.16),

$$dQ = r\left(\tfrac{1}{2}\right)\rho_\infty U^2 C\left\{C_l\sin\alpha - C_d\cos\alpha\right\} ds$$

$$dT = \left((\tfrac{1}{2})\rho_\infty U^2 C\right)\left[\left\{\sin\beta\,\sin\phi\,(C_l\cos\alpha + C_d\,\sin\alpha)\right\} - \cos\phi\,(C_l\,\sin\alpha - C_d\,\cos\alpha)\right\}\right] ds$$

Let $C_t = C_l\,\sin\alpha - C_d\,\cos\alpha$ and (4.16a)

$$C_n = C_l\cos\alpha + C_d\,\sin\alpha \quad (4.16b)$$

where, C_t and C_n are tangential and normal force coefficients respectively.

Hence , $dQ = r(1/2)\rho\,U^2\,C\,C_t\,ds$

and, $dT = (1/2)\rho\,U^2\,C\,(\sin\beta\,\sin\phi\,C_n - \cos\phi\,C_t)\,ds$

Using Eqn. (4.11) , the above eqns. become

$$dQ = r(1/2)\rho\,U^2\,C\,C_t\,\frac{dz}{\sin\beta}$$

and, $$dT = (\tfrac{1}{2}\,\rho\,U^2\,C)(\sin\beta\,\sin\phi\,C_n - \cos\phi\,C_t)\,\frac{dz}{\sin\beta}$$

Therefore, the mean power and mean thrust produced by the lower half blade of Fig.(4.4) are found by integrating and averaging the above equations over interval 0 to 2π and also integrating from $z = -z_1 = -2b\,\sin\beta$ to $z = 0$. Thus

$$P_{hb} = \frac{1}{2\pi} \int_{-z_1}^{0} \int_{0}^{2\pi} r\Omega \left(\frac{1}{2}\right) \rho_\infty U^2 C \, C_t \, \frac{d\phi \, dz}{\sin\beta} \quad \text{and}$$

$$T_{hb} = \frac{1}{2\pi} \int_{-z_1}^{0} \int_{0}^{2\pi} \left(\left(\frac{1}{2}\right) \rho_\infty U^2 C\right) \left[\sin\beta \, \sin\phi \, C_n - \cos\phi \, C_t\right] \frac{d\phi \, dz}{\sin\beta}$$

where the subscript hb signifies value for half-blade. Since each blade has two equal half blades, for the mean power and mean thrust of the whole wind turbine, the above expressions are to be multiplied by 2N, where N is the number of blades. Thus the mean power and mean thrust of a wind turbine can be expressed as follows :

$$P = - \frac{N}{\pi} \int_{0}^{-z_1} \int_{0}^{2\pi} r\Omega \left(\frac{1}{2}\right) \rho_\infty U^2 C \, C_t \, \frac{d\phi \, dz}{\sin\beta} \quad \text{and} \qquad (4.17)$$

$$T = - \frac{N}{\pi} \int_{0}^{-z_1} \int_{0}^{2\pi} \left(\left(\frac{1}{2}\right) \rho_\infty U^2 C\right) \left[\sin\beta \, \sin\phi \, C_n - \cos\phi \, C_t\right] \frac{d\phi \, dz}{\sin\beta} \qquad (4.18)$$

If we define the solidity σ, the local tipspeed ratio λ', local power coeff. C_P' and local thrust coeff. C_T' as follows :

$$\sigma = \frac{N \, C}{R} = \frac{N \, C}{R'} \, f_1 \qquad (4.19a)$$

$$\lambda' = \frac{\Omega R}{V} = \frac{\Omega R'}{V f_1} \qquad (4.19b)$$

$$C_P' = \frac{P}{(1/2)\ \rho_\infty A' V^3} \qquad (4.19c)$$

$$C_T' = \frac{T}{(1/2)\ \rho_\infty A' V^2} \qquad (4.19d)$$

It is to be noted that C_P' and C_T' have been defined for reefed case based on the local speed V and therefore, area A' has been used for non - dimensionalization . Earlier, Selvaraj (1992) used the area A, i.e., unreefed intercepted area of wind turbine , for non-dimensionalization, i.e., he used the following definition of C_P' and C_T' ----

$$C_P' = \frac{P}{(1/2)\rho_\infty A V^3} \quad \text{and} \quad C_T' = \frac{T}{(1/2)\rho_\infty A V^2}$$

But, as it is obvious that as the wind turbine reefs, the intercepted area decreases resulting in a decrease in absorbed power and hence decrease in power coefficient. Therefore, the area A' has been used for non-dimensionalization of C_P' and C_T' as in Eqns.(4.19c & 4.19d) to take into account this fact. Selvaraj's analysis does not incorporate this fact because he had used area A for non-dimensionalization of C_P' and C_T' even in reefed case.
Here C is the chord, and N is the number of blades .
Normalising the rotor area by R, we have

$$k_1 = \frac{A}{R^2} = \frac{A'}{f_2} \left(\frac{f_1}{R'}\right)^2 \qquad (4.20)$$

Using the Eqns.(4.19) & (4.20) in Eqn.(4.17) and dividing both sides of Eqn.(4.17) by $(1/2\ \rho_\infty A' V^3)$, we get

$$\frac{P}{1/2\ \rho_\infty A' V^3} = -\frac{NC}{\pi} \int_0^{-z_1} \int_0^{2\pi} \frac{r\ \Omega\ 1/2\ \rho_\infty U^2 C_t}{1/2\ \rho_\infty A'\ V^3} \frac{d\phi\ dz}{\sin\beta}$$

or

$$C_{P'} = -\frac{NC}{\pi R} \int_0^{-z_1} \int_0^{2\pi} \frac{r}{R} \frac{\Omega R}{V} \left(\frac{U}{V}\right)^2 \frac{d\phi}{\sin\beta} \frac{dz}{R} \frac{R^2}{A'} C_t$$

ie,

$$C_{P'} = -\frac{\sigma\lambda'}{\pi\ k_1} \int_o^{-\bar{z}_1} \int_o^{2\pi} \bar{r}\ (U/V)^2\ C_t \frac{d\phi\ d\bar{z}}{\sin\beta\ f_2} \qquad (4.21)$$

Similar deduction can be done for C_T' also and we finally arrive at the expression for C_T' as

$$C_{T'} = -\frac{1}{\pi k_1} \int_0^{-\bar{Z}_1} \int_0^{2\pi} \sigma (U/V)^2\ (\sin\phi\ \sin\beta\ C_n - \cos\phi\ C_t) \frac{d\phi\ d\bar{z}}{f_2 \sin\beta}$$

(4.22)

where $(U/V)^2 = (\bar{r}\lambda' + \cos\phi)^2 + (\sin\phi\ \sin\beta)^2$ (4.23)

Also Eqn.(4.14),after using Eqn.(4.19) becomes,

$$\tan \alpha = \frac{\sin \beta \sin \phi}{\bar{r} \lambda' + \cos \phi} \qquad (4.24)$$

The above expressions namely, Eqns.(4.21) & (4.22) will now be converted in terms of useful (true) tipspeed ratio (λ) by using Eqn.(2.23). The detailed analysis was done by Shankar [1976], which avoids iterative procedure while calculating $C_P$and C_T. Thus,

$$\lambda = \lambda' (V/V_\infty) = \frac{\lambda'}{(1 + C_T'/4)} \qquad (4.25)$$

$$C_P = C_P' (A'/A) (V/V_\infty)^3 = \frac{C_P' f_2}{(1 + C_T'/4)^3} \qquad (4.2$$

$$C_T = C_T' (A'/A) (V/V_\infty)^2 = \frac{C_T' f_2}{(1 + C_T'/4)^2} \qquad (4.2$$

The mean torque coefficient, C_Q may be deduced from C_P as follows.

$$C_P = \frac{Q \Omega}{1/2 \rho_\infty A V_\infty^3} = \frac{Q}{1/2 \rho_\infty A V_\infty^2} \frac{\Omega R}{V_\infty R}$$

ie $C_P = C_Q \lambda$

Hence $C_Q = \frac{C_P}{\lambda}$ (4.28)

where $C_Q = \dfrac{Q}{1/2\ \rho_\infty\ A\ V_\infty^2 R}$ (4.29)

We note that for blades symmetrically curved about an of radius R′ with const. chord and of symmetrical section, Eqns. (4.21) & (4.22) reduce to

$$C_P' = -\frac{2\sigma\lambda'}{\pi\ k_1} \int_0^{-\bar{z}_1} \int_0^{\pi} (U/V)^2\ \bar{r}\ C_t\ \frac{d\phi\ d\bar{z}}{\sin\beta\ f_2} \qquad (4.30)$$

$$C_T' = -\frac{2\sigma}{\pi\ k_1} \int_0^{-\bar{z}_1} \int_0^{\pi} (U/V)^2\ (\sin\phi\ \sin\beta\ C_n - \cos\phi\ C_t)\ \frac{d\phi\ d\bar{z}}{\sin\beta\ f_2} \qquad (4.31)$$

From Eqn. (4.1b) , we have

$$\frac{b}{R} = 0.9\ \tan\theta_o$$

Also, $k_1 = \dfrac{A}{2} = \dfrac{8\ Rb}{2} = 7.2\ \tan\theta_o$

Therefore, Eqns. (4.30) and (4.31) become

$$C_P' = -\frac{\sigma\ \lambda'}{3.6\pi\ \tan\theta_o} \int_0^{-\bar{z}_1} \int_0^{\pi} (U/V)^2\ \bar{r}\ C_t\ \frac{d\phi\ d\bar{z}}{\sin\beta\ f_2} \qquad (4.32)$$

$$\& \quad C_T' = -\frac{\sigma}{3.6\pi\ \tan\theta_o} \int_0^{-\bar{z}_1} \int_0^{\pi} (U/V)^2 (\sin\phi\ \sin\beta\ C_n - \cos\phi\ C_t) \frac{d\phi\ d\bar{z}}{f_2 \sin\beta} \qquad (4.33)$$

where $-\bar{z}_1 = -z_1/R = -\dfrac{2b\ \sin\beta}{R} = -1.8\ \tan\theta_o\ \sin\beta$

4.1.5 Aerodynamic Forces :

Load distribution along the span of the blade is necessary for structural design of the blade. These forces are nothing but the tangential and normal forces acting on the blade.
The tangential force per unit length of the blade is given by

$$F_c(\phi) = 1/2\ \rho_\infty\ U^2\ C_t\ C \qquad (4.34)$$

and the normal force per unit length of the blade is given by

$$F_n(\phi) = 1/2\ \rho_\infty\ U^2\ C_n\ C \qquad (4.35)$$

Now Eqn.(4.34) can be written as

$$F_c(\phi) = 1/2\ \rho_\infty \left(U/V_\infty\right)^2 V_\infty^{\ 2}\ C_t\ C \qquad (4.36)$$

Similarly, the normal force becomes

$$F_n(\phi) = 1/2\ \rho_\infty \left(U/V_\infty\right)^2 V_\infty^{\ 2}\ C_n\ C \qquad (4.37)$$

Thus for a given freestream velocity, V_∞, if the parameter $(U/V_\infty)^2$ is known then the aerodynamic forces can be evaluated. The expression for the above parameter may be deduced as follows.

$$\left(U/V_\infty\right)^2 = \left(U/V\right)^2 \left(V/V_\infty\right)^2 \qquad (4.38)$$

where $(U/V)^2$ is given by the Eqn.(4.23) and

$$\left(V/V_{\infty}\right)^2 = \left(\lambda/\lambda'\right)^2 .$$

Note that the normal force is positive for $0 \leq \phi \leq \pi$ and negative for $\pi \leq \phi \leq 2\pi$.

CHAPTER - 5

Results and Discussion :

The primary interest of the present work is to evaluate the aerodynamic characteristics of VGVAWT and the aerodynamic loads acting on the blade of VGVAWT.

The VGVAWT has the following specifications :

Elevation = 20 m

Rotor radius R = 4.5 m

Rotor area A = 58.5 m^2

Blade length = 6.5 m

Chord length (C) = 0.45 m

No. of blades (N) = 2

Solidity σ = 0.2

$(V_\infty)_{rated}$ = 10 m/s

$(C_P)_{rated}$ = 0.42

$(\lambda)_{rated}$ = 4

$(Power)_{rated}$ = 10 kW

$(\Omega)_{rated}$ = 85 rpm

Airfoil used : NACA 0012

The eqns. (4.32) and (4.33) have been solved numerically using a FORTRAN program which has been developed. The values of C'_P and C'_T were obtained for various values of λ' for a given value of β. Then the eqns. (4.25), (4.26), (4.27) and (4.28) are used to calculate λ, C_P, C_T and C_Q. NACA 0012 airfoil has been used for the computation. The section characteristics (C_l and C_d) have been adopted from Ref. [5] and reproduced in Figs. (5.1 a) and (5.1 b). These characteristics were obtained experimentally for Re. No. =

0.3×10^6 . The Re. No. for the present case is 0.38×10^6, corresponding to V_∞ = 10 m/s and hence the use of the above data is justified.

In Fig.5.2 , the variations of C_P, C_T and C_Q with λ are presented for $\beta = 90^0$. C_P is maximum at tipspeed ratio (λ) = 4 and this value is 0.52 . For values of λ less than 0.8, C_P is close to zero. After that it rises with λ till λ = 4.0 and then, it starts decreasing afterwards. At λ = 0, C_T has a non - zero value of 0.125 and it increases with λ. C_T approaches to a value = 1.0 asymptotically over the range of tipspeed ratios from 6 to infinity. Also, $(C_Q)_{max}$ = 0.15 occurs at λ = 3.2, before $(C_P)_{max}$ occurs.

The Figs.5.3 ,5.4 ,5.5 and 5.6 show the variation of C_P, C_T, C_Q and (V/V_∞) with the arrowhead angles respectively. Also the results of Selvaraj(1992) have been overlapped for comparison . It is to be noted that for lower tipspeed ratios (near λ = 0), the curves of C_P, C_T, C_Q & V/V_∞ for the present case and for Selvaraj overlap. For higher tipspeed ratios, Selvaraj's analysis overpredicts the values of C_P, C_T, C_Q & V/V_∞ compared to the present analysis.

From Fig.5.3 , it is obvious that decrease in arrowhead angle, or in other words, increase in reef angle results in decrease in maximum power coefficient for both Selvaraj and the present case (Pandey, 1996) which is obvious because the decrease in arrowhead angle will decrease the intercepted area thereby reducing the absorbed power. The max. power coefficient occurs at a lower tipspeed ratio when the arrowhead angle is decreased for the present case. For a given arrowhead angle, the max. power coefficient occurs at a lower tipspeed ratio for the present case

than that for Selvaraj's case. The smaller the β the more flattened is the curve and C_p goes to zero at a higher tipspeed ratio than the rated tipspeed ratio $(\lambda)_{rated} = 4.0$ for both the cases.

The Fig.5.4 shows that C_T has a value of 0.12 at $\lambda = 0$ and it starts increasing with increasing tipspeed ratio for $\beta = 90^\circ$ for both the cases i. e. the present case and the Selvaraj's case. For other values of β, C_T also increases with increasing λ .The value of C_T at the zero tipspeed ratio decreases with decrease in arrowhead angle for both the cases

Fig.5.5 shows that at $\lambda = 0$, the starting torque coefficient C_Q is 0.026 for $\beta = 90^\circ$ and it starts decreasing with decrease in β for both the cases.

Fig.5.6 shows that the velocity ratio (V/V_∞) decreases with tipspeed ratio for a given β for both the cases. At zero tipspeed ratio, (V/V_∞) increases and approaches towards 1.0 as β is decreased.

For $\beta = 90^\circ$, (V/V_∞) is 0.97 and for $\beta = 30^\circ$, it is 0.99 for the present case as well as for Selvaraj.. For $\beta = 90^\circ$, (V/V_∞) decreases much faster with λ than for $\beta = 30^\circ$.

The effect of solidity on C_p is given in the Fig.5.7. The decrease in solidity shifts the curve towards right and also the curve becomes more and more flattened near the maximum. The increase in solidity shifts the $(C_p)_{max}$ towards lower tipspeed ratio. There exists an optimum solidity (between 0.2 and 0.3) for which the power coefficient is max. for $\beta = 90^\circ$. Shankar's calculations (non - uniform induced velocity approach) have been superimposed for comparison. It is found that the present theory overpredicts the maximum power coefficient.

Fig.5.8 shows the angle of attack variation of the blade with azimuthal position for different tipspeed ratios ($\beta = 90^\circ$). It is obvious that for zero tipspeed ratio, the angle of attack, α, is same as ϕ and that's why we get a straight line showing $\phi = \alpha$ for $\lambda = 0$. Note that the blades stall for tipspeed ratios from 0 to 2.3, the stall angle being 14°. The variation of α with ϕ varying from 180° to 360° is obtained by double reflection of this graph, first about vertical plane ($\phi = 180^\circ$) and then about horizontal plane ($\alpha = 0^\circ$)

Figs.5.9 and 5.10 show the variation of the tangential and normal force coefficients, C_t and C_n, respectively as functions of azimuthal angle (ϕ) for various tipspeed ratios (for $\beta = 90^\circ$). The results have been plotted for a single blade. For $\lambda = 0$, the value of C_t is -0.013 for the blade at $\phi = 0$ and 0.013 for the second blade at $\phi = 180^\circ$.

For computing the tangential force and normal force per unit length of the blade, we need to calculate the value of $(U/V_\infty)^2$ and hence, it is also computed and plotted in the Fig.5.11. Note that the aerodynamic forces acting on the blades are greatest for the unreefed condition, therefore C_t, C_n and $(U/V_\infty)^2$ are computed only for $\beta = 90^\circ$.

In 1983, Mathews experimentally obtained power coefficients of 25 m VGVAWT for different reef angles. This has been compared with Selvaraj and the present analysis as shown in Fig.5.12 . From Fig.5.12 , it is obvious that for $\beta = 90^\circ$, the 25 m VGVAWT has $(C_p)_{max} = 0.45$ at the tipspeed ratio 3.5 whereas the present and the Selvaraj's 20 m VGVAWT has $(C_p)_{max} = 0.52$ at tipspeed ratio 4. This discrepancy may be due to the assumption of uniform disc velocity (V) in the present theory. Hence, we can say that the

present theory overpredicts the max. power coefficient. But, the results of present theory are more closer to Mathews' experimental results than that of Selvaraj's (Fig. 5.12). Hence the present analysis gives more reliable results than that of Selvaraj's analysis (1992). Note that for $\beta = 90^{\circ}$, the present analysis and the Selvaraj's analysis give the same results.

From Fig.5.7 , one can infer from the graphs obtained by Shankar [1976] that the uniform disc velocity theory (present case) overpredicts the max. power coefficient by about 10% when the solidity ratio is 0.2.

Also we can observe that the increase in the reef angle (i. e. the decrease in the arrowhead angle) results in decrease in $(C_p)_{max}$ in all the cases (Mathews, Selvaraj and present case, Fig.5.12), but C_p goes to zero at a lower tipspeed ratio in the case of 25 m VGVAWT (Mathews) whereas C_p goes to zero at a higher tipspeed ratio, for the present case and for Selvaraj's case. This may be due to the fact that the 25 m VGVAWT reefs without extending radially outward , thereby producing more rapid decrease in swept area which results in rapid decrease in C_p with λ. But, the present case VGVAWT has a special feature of extending radially outward when it reefs. This feature decreases the swept area gradually and hence C_p becomes more and more flattened near the maximum as reef angle is increased.

Conclusions & Recommendations:

1. The results of present theory (refer C_P vs λ curve of Fig. 5.12) are closer to Mathews' experimental results than that of Selvaraj's results. Hence, the present analysis improves over Selvaraj's analysis.
2. Selvaraj's analysis overpredicts the values of C_P, C_T, C_Q and (V/V_∞) compared to the present analysis.
3. The present analysis and the Selvaraj's analysis have assumed the blade to be having 2-D characteristics all along the span. The analysis can be repeated by considering the blade as a wing to improve the results.
4. Present analysis and Selvaraj's analysis have adopted the uniform induced velocity approach. Future work can be done by adopting non-uniform induced velocity approach to improve the results.

CHAPTER - 6

Summary of the work done on VGVAWT at I.I.T. Kanpur

6.1 Introduction

The potential of Vertical Axis Wind Turbine (VAWT) was recognised in the early seventies. Since then development of this wind turbine has witnessed many changes. The variable geometry VAWT was investigated and tried out in the UK. A 17m diameter 100 kW variable geometry VAWT was set up in the Isle of Scilly (Mays et al 1987). This turbine had an active control system. Active control systems depend upon transducers to sense wind speed, rpm, reef angle etc. whereas the passive control systems do their own sensing. These transducers must be very rugged, weatherproof and reliable and thus active control systems are expensive (also they tend to be quite sensitive to lightning and coastal regions in the tropical and sub - tropical parts of the globe are lightning - prone). In late 1987, there was a failure in the control system in the turbine of Scilly Isle which led to an overspeed situation causing damage (Mays 1989, Lindley 1988/89).

The variable geometry rotor was given up in favour of the fixed geometry passive control (stall regulated) rotor (Lindley,1989). In a VAWT the blade aerodynamic load alternates in direction (radially inward and outward) and hence the more severe loads in a stall regulated fixed geometry rotor would lead to greater fatigue. Ghosh (1990) predicted quite early that the fixed geometry rotor may not survive in a coastal area swept frequently by cyclones and tornadoes. Wind speeds in a tornado range from 110 to 550 km/hr and those in a cyclone from 180 to 280 km/hr (Sachs,

1972). As it so happens, the fixed geometry VAWT in the UK, a region which has milder storms, shed blades due to structural failure (Page, 1991) and the VAWT program there is now on hold.

The variable geometry VAWT subjects its blades to lesser loads and enjoys certain advantages especially in the coastal regions of the tropical and sub-tropical parts of the world swept by cyclones. In these regions, a Wind Turbine(WT) harnesses a slightly inferior average wind compared to the temperate zone (near 40° latitude) but must survive the tremendous wind speeds of a cyclone (Hurricane, Typhoon etc.). Ghosh (1990) proposed a new method of passive control system called Centrifugal Reef Control which is likely to be reliable and cost-effective for the variable geometry VAWT. A passive control system has the added advantage of not being susceptible to lightning strikes.

A prototype design project for a variable geometry VAWT with centrifugal reef control has been underway at I.I.T. Kanpur since 1993. This project is assisted by a grant from the Ministry of Non-conventional Energy Sources (MNES), Govt. of India. Various aspects of this design are presented here.

6.2 Rotor Design

6.2.1 Control and Aerodynamics

The wind turbine rotor assembly, as proposed by Ghosh (1990), consists of two telescopic cross-arms, each of which supports two half blades on one end (Fig. 6.1, the half blades are attached to an end plate which in turn is hinged to the cross-arm head). The other end of the cross-arm is connected to the rotor axis through a spring. Each half blade is connected via a control

strut to the sleeve which houses the telescopic cross-arms . The reef control mechanism is based on the centrifugal action wherein the centrifugal force acting on the blade cross-arm assembly is conterbalanced by a horizontal spring restraint. Any increase in wind speed beyond the rated speed leads to an increase in the wind turbine rpm above the rated rpm. This will increase the centrifugal force on the blade cross-arm assembly. As a result, the spring restraint is overcome and the cross-arm moves radially outwards and the blades reef to resemble an arrowhead. The net effect is to reduce the intercepted area and the component of the wind in the plane of the blade section, and thereby control the power output.

The preliminary aerodynamic investigation of a VAWT with centrifugal reef control to produce a power of 10 kW in 10 m/s wind has been carried out. Airscrew theory (commonly applied for aircraft propellers) in modified form has been used to compute power coefficient . Earlier, the power and thrust coefficients were computed for various reef positions (given by arrowhead angle β in Fig. 6.1) by Selvaraj (1992) using unreefed intercepted area (corresponding to $\beta = 90^{\circ}$) for non-dimensionalization. That means, he used power and thrust coefficients defined as follows -

$$C_P' = \frac{P}{(1/2)\rho_\infty A V^3} \quad \text{and} \quad C_T' = \frac{T}{(1/2)\rho_\infty A V^2}$$

where, P = power extracted from intercepted area

T = thrust acting on the wind turbine

ρ_∞ = free stream air density

A = unreefed intercepted area of wind turbine (for $\beta = 90^{\circ}$).

V = air velocity at the wind turbine

He used this definition even for $\beta < 90^{\circ}$ and got the power coefficient variation with various arrowhead angles as shown in Fig.5.3. The analysis has been repeated by Pandey(1996) using reefed intercepted area (A') for non-dimensionalization of C_P' and C_T' as follows -

$$C_P' = \frac{P}{(1/2)\rho_\infty A' V^3} \quad \text{and} \quad C_T' = \frac{T}{(1/2)\rho_\infty A' V^2}$$

where, A' = reefed intercepted area of wind turbine (for $\beta < 90^{\circ}$).

Obviously, for $\beta = 90^{\circ}$, A' = A.

The above definition results in greater values of C_T' for any given β and thus, by virtue of Eqn.(2.23), lesser values of V/V_∞. This in turn leads to smaller power.

Using this definition of power coefficient, the variation of power coefficient with different arrowhead angles has been evaluated, using a Fortran Code, and the results are shown in Fig.5.3 . On comparison , we see that the analysis of Selvaraj slightly overestimates the power coefficient.

6.2.2 Structure and mechanical configuration

The design of such a wind turbine requires an appropriate mass distribution such that the telescopic cross-arm is much heavier (about 2.5 times) than the rotor half blade (Ghosh ,1990). It further involves estimation of centrifugal force and an assesment of the spring stiffness capable of withstanding the centrifugal force for different reef angles.

The major dimensions of the wind turbine have been shown in Fig.3.1 . A detailed design study is carried out to determine the

size and relative position of various components of the rotor assembly. Fig.6.2 shows various features such as the bearing pads, spring, sleeve, cross-arm, end plate, blades etc.

One end of the control strut is hinged at the C G of the half blade. The sleeve, which houses the cross-arm and spring, has a box beam structure with taper over the inner radius portion. The cross-arm weighing approximately 55 kg is made of commercially available standard aluminium tubes. It is given a tubular structure to facilitate support by boundary lubricated bearing pads made of cast iron. Since aluminium offers a poor bearing surface, it is to be coated with tin through a chemical process (Horn,1967). Fig.6.3 shows the top view of the cross-arm which consists of two aluminium tubes placed side by side. Also the figure shows the Z - link which is connected onto the cross-arm by means of a fork [inset of Fig.6.3]. The purpose of the Z - link is to limit to and fro motion caused by the reversal of aerodynamic load on each blade and help maintain symmetry about the axis of rotation. The rotor half blade (NACA 0012 airfoil section) which is 3.25 m long, has a chord of 0.45 m and a rectangular planform. It weighs approx. 22 kg. The blade has an FRP composite structure, consisting of a skin wrapped over a D - spar, meant to withstand fatigue (Fig.6.4). It is provided with discretized internal taper to reduce weight and bring C G closer to the end plate (Fig.6.4). It carries a max. normal and tangential aerodynamic loads of 480 N/m and 80 N/m respectively. The detailed load calculations have been carried out by Selvaraj (1992) for the unreefed case of operation of wind turbine because the aerodynamic loads would be maximum for unreefed case and therefore, other reefed conditions would be automatically taken care of. Fig.6.5 shows the variation of the centrifugal force per

unit mass of the half blade with cross-arm movement as it reefs. The location of C G of cross-arm (denoted by r in Fig.6.6) for the unreefed case is 1.621 m from the axis of rotation (Ref. 33).

Fig.6.5 shows clearly that the centrifugal force is only slightly non-linear with r. Analysis reveals that for the present case, a stiffness of 0.4 kgf/mm is required for each spring in the pair to withstand the centrifugal force for different reef angles. The max. displacement of the cross-arm between unreefed and fully reefed conditions is 1.7 m. The springs are stretched by 0.8 m, even in the unreefed position. Hence, they have to undergo a total elongation of 2.5 m. Such special springs are made by a firm called Stumpp Schuele & Somappa Ltd. of Bangalore. The chosen spring has a free length of 3.0 m and weight of 58 kg. The elongation in the spring due to the centrifugal forces generated by its own mass is approximately 8.0 mm. However, this elongation may increase from 8.0 mm to about 16.0 mm in fully reefed condition (see Appendix 1, taken from ref. 32).

Now, we can summarise the wind turbine specifications as :

Unreefed radius R = 4.5 m

Rated tip speed ratio λ = 4

Rated angular velocity ω_o = 85 r p m

Half blade length L_b = 3.25 m

Blade chord length C_b = 0.45 m

Rated wind speed = 10 m/s

Cut in wind speed = 4 m/s

The wind turbine has no cut out wind speed, since at extremely high wind conditions the blades can reef by almost 90 deg., and still produce power. Other wind turbine characteristics are :

Mass of the half blade M_b = 22 kg

C.G. location of the half blade (Fig.6.6) cg_b = 1.3 m

Width of the end plate W_{ep} = 150 mm

Thickness of the end plate t_{ep} = 15 mm

Length of the end plate L_{ep} = 0.45 m

Mass of the end plate M_{ep} = 1.0 kg

Width of the sleeve W_{sl} = 175 mm

Thickness of the sleeve t_{sl} = 10 mm

Height of bearing sleeve or pad h_{sl} = 20 mm

Space between the bearings , bear_s = 1.5 m

Location of the strut hinge X_h = 2.0 m

Location of the near end of X-arm (Unreefed) X_x = 150 mm

Mass of the X - arm M_x = 55 kg

The following work was done by J. Singh (Ref. 33) and the same is being presented here.

6.3 Dynamics & Response

The purpose of dynamic analysis is to study the transient response of the reefing blades of wind turbine and see how quickly they settle down to their new equilibrium position at increased wind speeds. The approach is to determine the changes taking place along the blade's trajectory. To evaluate the increased rpm and formulate the dynamic equations, we trace the motion of the wind turbine blade, starting at some value of the azimuth angle ϕ .

Let the wind turbine blade be at station 0 at time t = 0 when the azimuth angle $\phi = \phi_o$ (Fig.6.8). The subscript 0 is used to denote quantities at station 0 at t = 0. The wind velocity V_o at the actuator disc can be obtained from the ratio (V/V_∞) which is a function of arrowhead angle β and the tipspeed ratio λ (refer to Fig.5.6). Let us assume that there is a sudden jump in the free stream wind velocity at station 0 from 10 m/s to 11 m/s (i.e. unit step jump). This increase in free stream wind velocity will result in a corresponding increase in the wind velocity at the disc.

Knowing β & λ , this increased V at station 0 (denoted by V_j) at the disc can be evaluated in the following way (from Fig.5.6) : (These values have been taken from Selvaraj's work(1992) for reefed as well as unreefed case of wind turbine operation because his analysis would give conservative structural as well as dynamical design and hence these values have been taken) .

For V_∞ = 10 m/s, $\lambda = \omega_o R / V_\infty$ = 4.0, β = 90° gives V_o / V_∞ = 0.72 .....(1)

For V_∞ = 11 m/s, $\lambda = \omega_o R / V_\infty$ = 3.64, β = 90° gives V_j / V_∞ = 0.74 .....(2)

where, subscript j denotes the variable after the jump. The ratio V_j/V_∞ = 0.74 is assumed to be constant for the calculations performed at all the subsequent values of azimuth angles and arrowhead angles. The increase from V_o to V_j will modify the velocity triangle at station 0 and consequently, the angle of attack increases from α_o to α_j (enlarged view of inset in Fig. 6.8) and there is a corresponding increase in the aerodynamic torque from Q_o to Q_j . At rated wind speed conditions, the average aerodynamic torque over a cycle is equal to the generator torque Q_g and the blades rotate at a constant rpm. With the jump in the aerodynamic torque from Q_o to Q_j , the net increase given by (Q_j - Q_g) causes the wind turbine to accelerate to increased angular velocity.

To determine the aerodynamic torque Q_{hb} produced by the half blade, we divide the half blade into N number of equal segments, with the i^{th} segment being located at a distance l_i from the end plate and r_i from the axis of rotation (Fig.6.9).

Then,

$$Q_{hb} = (1/2)\rho_\infty (L_b/N) C_b \sum_{i=1}^{N} U_i^2 \, r_i (C_t)_i \quad \ldots\ldots (3)$$

where, C_t = tangential force coefficient

ρ_∞ = free stream density

L_b = half blade length

C_b = blade chord

U_i = relative velocity of the i^{th} blade segment in the plane of the blade section.

The aerodynamic torque Q produced by a single wind turbine blade is given by ----

$$Q = 2Q_{hb} \quad \ldots\ldots (4)$$

Hence, $$Q = \rho_\infty (L_b/N) C_b \sum_{i=1}^{N} U_i^2 \, r_i (C_t)_i \quad \ldots\ldots (5)$$

where, $$r_i = R' - l_i \cos\beta \quad \ldots\ldots (6)$$

R' = reefed wind turbine radius (Fig.6.7)

$$= X_h + L_s \cos\theta_s + cg_b \cos\beta \quad \ldots (7)$$

where, $$\theta_s = \sin^{-1} [\{W_{ep} \cos\beta/2 + (cg_b + t_{ep}) \sin\beta + h_z\}/L_s] \quad \ldots (8)$$

The distance l_i of the i^{th} segment from the end plate is

$$l_i = (L_b/N) \ (i - 1/2) \quad \ldots\ldots (9)$$

The wind speed U_i contributing to the torque Q is given by

$$U_i^2 = (r_i \omega + V \cos\phi)^2 + (V \sin\phi \sin\beta)^2 \quad \ldots\ldots (10)$$

The tangential force coefficient (C_t) for the i^{th} blade segment is given by --

$$(C_t)_i = C_l \sin\alpha_i - C_d \cos\alpha_i \quad \ldots (11)$$

where, $$\alpha_i = \tan^{-1} [V \sin\beta \sin\phi \ / \ (r_i \omega + V \cos\phi)] \quad \ldots\ldots (12)$$

C_l and C_d are the section lift and drag coefficients.

The aerodynamic torque Q_{o1} and Q_{j1} for the first blade at station 0 can now be calculated by the use of equations (4 - 12) as

$$Q_{o1} = \rho_\infty (L_b/N) \ C_b \sum_{i=1}^{N} [U_i^2]_o \, r_i [(C_t)_i]_o \quad \ldots\ldots (13)$$

$$Q_{j1} = \rho_\infty (L_b/N) \ C_b \sum_{i=1}^{N} [U_i^2]_j \, r_i [(C_t)_i]_j \quad \ldots\ldots (14)$$

Similarly, the aerodynamic torques Q_{o2} and Q_{j2} for the second blade can be obtained by computing α_i, U_i and $(C_t)_i$ for $180 + \phi$. The total aerodynamic torques Q_o and Q_j produced by the wind turbine are then given by --

$$Q_o = Q_{o1} + Q_{o2}$$

$$Q_j = Q_{j1} + Q_{j2}$$

The net increase in the aerodynamic torque at station 0 which causes the wind turbine to accelerate to an increased rpm is given by ---

$$\Delta Q = Q_j - Q_g \quad \ldots\ldots (15)$$

If I denotes the sum total of the moment of inertia of all the components of the wind turbine rotor assembly, the angular acceleration $\ddot{\theta}$ is given by the following relation --

$$I\ddot{\theta} + 2\,[(2V_x\omega)\, M_x r'] + 2[4\omega \sum_{i=1}^{N} (V_x - l_i \dot{\Gamma}\, \mathrm{Cos}\Gamma) m_i r_i] = \Delta Q \quad \ldots(16)$$

The last two terms in the above expression arise due to the Coriolis effect of rotation.

Here, V_x = radial velocity of the X - arm

ω = angular velocity

l_i = distance measured from the end plate (Fig.6.10)

The Coriolis component of the acceleration for the X - arm is $2V_x\omega$. If M_x is the mass of the X - arm and r′ the location of the c.g. of the X - arm (r′ = r + T, where r is the c.g. location in unreefed condition and T is the travel or displacement of the X - arm; Fig.6.7), the expression within square brackets in the second term of above eqn. represents the negative torque arising out of the Coriolis acceleration of the X - arm, and hence it is included in the LHS of the eqn. This expression has been multiplied by a factor of 2 to account for both the X-arms .

The expression within square brackets in the third term of above eqn. represents the negative torque due to the Coriolis effect obtained for a single wind turbine blade. This term is more complex since the blade hinged to the end plate is moving outward with velocity V_x and at the same time it reefs through an angle Γ. If $\dot{\Gamma}$ is the angular velocity with which the blade is reefing, then $(V_x - l_i\dot{\Gamma}\ Cos\Gamma)$ gives the net velocity of the i^{th} segment in the radially outward direction. If m_i & r_i represent the mass and the distance from the axis of rotation of the i^{th} segment respectively, then the torque for a blade arising due to the Coriolis effect of rotation is given by

$$4\omega \sum_{i=1}^{N} (V_x - l_i\dot{\Gamma}\ Cos\Gamma)\ m_i r_i$$

This term has been multiplied by a factor of 2 in eqn.(16) to take into account both the blades of the Wind Turbine.

The moment of inertia I is the summation of the moment of inertia of all the rotating components of the wind turbine and is given by --

$$I = I_{blade} + I_{X\text{-}arm} + I_{sleeve} + I_{spring} + I_{end\text{-}plate} \quad \ldots\ (17)$$

For the angular velocity, $\omega = \omega_o, \beta = 90^0, \Gamma = 0, \dot{\Gamma} = 0$ and $V_x = 0$, eqns.(16) and (17) can be used to determine the angular acceleration $\ddot{\theta}$ at station 0 at time t = 0.

Let us assume that the blade reaches station 1 after time Δt = 0.1 sec (Fig.6.8). Then, the angular velocity at station 1 can be obtained as --

$$\omega_1 = \ddot{\theta}\ \Delta t + \omega_o \qquad \ldots.(18)$$

The new azimuth angle at station 1 is given by -----

$$\phi_1 = \{(\omega_1 + \omega_0)/2\}\Delta t + \phi_0 \quad \ldots..(19)$$

The angular velocity increases from ω_o at station 0 to ω_1 at station 1. This causes an increase in the centrifugal force thereby setting the X - arm in motion. Obviously, the reefing

comes into play only from station 1 onwards.Hence, at station 1, the arrowhead angle β is still equal to 90°. For β = 90° and ϕ = ϕ_1, eqns. (4 - 12) can be used to evaluate the torque Q_1 at station 1.

Now, let us assume that the blade takes time Δt to move from station 1 to station 2 (Fig.6.11). The increased aerodynamic torque which causes the angular acceleration from station 1 onwards is given by --

$\Delta Q = Q_1 - Q_g$ ....(20)

where, Q_1 = aerodynamic torque at stn. 1

Q_g = generator torque

For the value of ΔQ given by eqn.(20), β = 90 deg. and V_x = 0, the angular acceleration $\ddot{\theta}$ at station 1 can be calculated by eqn.(16). Since the wind turbine blades are reefing, there is a continuous change in the aerodynamic torque and angular acceleration from stn.1 onwards. To evaluate this variation in torque and angular acceleration during the blade's motion from stn.1 to stn.2, we divide Δt (Fig.6.11) into small time intervals each of magnitude δt (assume δt = 0.01sec). Obviously, the blade starting from stn.1 reaches stn.1_1 in time δt. In this time δt, the blades reef through a certain angle Γ and the c.g. of the X - arm experiences a displacement x in the radial outward direction. We have to obtain the values of Γ and x at station 1_1 which will subsequently yield the value of the torque Q_{1_1} at station 1_1. The change in the aerodynamic torque ΔQ ($\Delta Q = Q_{1\_1} - Q_g$) can then be evaluated and used to calculate the value of the angular acceleration $\ddot{\theta}$ at station 1_1. Starting from station 1, the various steps involved in arriving at the values of ΔQ_{1_1} and $\ddot{\theta}$ at station 1_1 are similar as involved in going from stn.0 to stn.1.

We keep on repeating this process from stn. to stn. till the arrow head angle β stabilizes to some value for all the following stations and the difference in the rated and the final angular velocity (corresponding to the new equilibrium value of β) is not more than 1%.

Based on the above formulation, the response of the wind turbine rotor assembly to a step jump in the wind velocity was observed.We took Selvaraj's result for load calculation even for $\beta < 90^{\circ}$ because it would give conservative dynamical prediction. The free stream velocity was assumed to increase from 10 m/s to 11 m/s and the time history of ω and β was plotted. Fig.6.13(a) shows ω (in rad/s) plotted against time (in sec.). The cyclic variation in ω observed in the graph is due to the variation in torque along the path traced by the turbine blades. It is observed that the time period of the cyclic variation in ω decreases near the peak due to increased angular velocity. Fig.6.13(b) shows the value of rpm averaged over one rotation plotted against time. The mean rpm is observed to increase and then smoothly decrease to the rated rpm in a short span of time. Fig.6.14 shows the time history of arrowhead angle β. The response is observed to be critically damped and the arrowhead angle settles down to its new equilibrium value with practically no oscillations.

6.4 Grid connection and Starting

The turbine turns an induction generator which is connected to the grid. The principal advantage of the induction generator is its ability to draw power from the grid to start the turbine, which has a poor starting torque like most other VAWTs. When a wind speed of 4 m/s (equal to the cut in wind speed) persists for more

than 10 sec., a wind speed sensor activates the starting procedure. As told earlier, the WT has no cut out wind speed since at extremely high wind conditions the blades can reef by almost 90 degrees and still produce power.

REFERENCES

1. Abott H. IRA. (1958),
   ''Theory of wing sections'', Dover Publications Inc. NY.

2. Anderson M B, Groecchel K M and Powles SJR,
   ''Analysis of data from the 25 m VGVAWT'', BEWA Annual Conference, Edinburgh.

3. Baker, J.R. (1983),
   ''Features to aid or enable self - starting of fixed pitch low solidity VAWTs'', J. Wind Engg. & Ind. Aerodyn.,Vol.15 (1983), pp 369 - 380.

4. Carnahan BHA Luther and J O Wilkes,
   ''Applied Numerical Methods'', John Wiley, NY (1969).

5. Critzos, C C Heyson, H H & Boswinkle R W (1955),
   ''Aerodynamic characteristics of NACA 0012 airfoil section at angles of attack from 0° to 180°'', NACA Tech. Note 3361.

6. David M Eggleston and Forrest S. Stoddard (1987),
   ''Wind Turbine Engineering Design'', Von Nostrand Reinhold NY.

7. Ficence IP (1987),
   ''The VAWT and its Power Train Design'', Power Transmission CME, April 1987, pp 35 - 39.

8. Frerris L L (1990),
   ''Wind Energy Conversion Systems'', Prentice Hall NY.

9. Griffith R T (1987),
   ''The effect of aerofoil characteristics on wind mill

performance'', Aeronautical Journal , July 1977, pp 322 - 326.

10. Glauert H (1963),
''Airplane Propellers and Airscrew Theory'', Division - L Aerodynamic Theory, Edited by Durand W.F.,Dover Edition, NY.

11. Horn C.C., C. Engg. MIEE and A P Witten CAP Industry Ltd., Reading, Berks.
''A Control and Monitoring System for a wind turbine ——— A Practical Experience''.

12. Jagadeesh A (1988),
''Integration of wind farms into the public power system in India'', J. Wind Engg. & Ind. Aerodyn. Vol. 27 (1988), pp 433 - 438.

13. John Twidell and Tony Weir,
''Renewable Energy Resources'', Chapt. 9 - Power from the wind, pp 204 - 241.

14. Kunal Ghosh (1990),
''Centrifugal Reef Control of Variable Geometry Vertical Axis WindTurbine'',Proceedings of World Renewable Energy Congress Reading, U K, Sept.(1990).

15. Mathews D L (1983),
''25 m VGVAWT Feasibility Study'', Summary Report

16. Musgrove P J & Clare R (1987),
''Development of the U K Vertical Axis Wind Turbine '', Wind Power'87 Conference, San Francisco Oct. 1987.

17. Peter South & Raj Rangi (1973),

''The Performance & Economics of the Vertical Axis Wind Turbine developed at NRC Ottawa, Canada'', 1973, Annual meeting of the Pacific Northwest Region of the American Society of Agricultural Engg.

18. Ramesh A S (1989),
''Interaction of Aerodynamics with Reefing Controls of a Variable Geometry Vertical Axis Wind Turbine'', M. Tech. thesis, Deptt. of Aero. Engg. , I.I.T. Kanpur.

19. Rangi R S South P & Templin R J (1974),
''Wind Power and the Vertical Axis Wind Turbine Developed at the NRC''.

20. Satyanarayana B (1990),
''High Wind Power potential regions in India '', Energy & Environment into the 1990s, Vol. 3, pp 1770 - 1774.

21. Shankar P N (1976),
''Aerodynamic performance of Vertical Shaft Wind Mills'', Proceedings Royal Society of London
—— A Series No. 349, pp 35 - 51.

22. Sir Robert McAlpine & Sons Limited and NEI plc (1986),
''Vertical Axis Wind Turbine'', Technical Data, 1986.

23. Stewart H J,
''Dual optimum aerodynamic design for a conventional Wind Mill'', AIAA Journal, Vol. 14, No. 11, pp 1524 - 1528.

24. Templin R J (1974),
''Aerodynamic performance theory for NRC Vertical Axis Wind Turbine'', NRC Report .

25. Wilson & Lissamann,
''Applied Aerodynamics of Wind Power Machines''.

26. Ruddar Dutt & K P M Sundharam ,
''Indian Economy''. pp 100 - 101.

27. Lindley D., Ed.(1988/89),
''Scilly Isles gets new Turbine'', WINDirections, Vol.8,
No.3, pp 8-9.

28. Mays I. D., Morgan C. A. and McDonnell A. (1987),
''The Demonstration of a 17m diameter Vertical Axis
Wind Turbine''. pp 12-20, Elsevier Applied Science,
London and New York.

29. Musgrove P. J.(1976),
''The Variable Geometry Vertical Axis Windmill'',
Proceedings of International Symposium on Wind Energy
Systems, Cambridge.

30. Sachs P.(1972),
Wind Forces in Engineering, Pergamon Press, Oxford.

31. Page, D. I.(1991),
UK review of wind energy activities during 1990/91,
In : DC Quarton and VC Fenton (Eds) Wind Energy Conversion,
pp 15-20.

32. ''Report on VGVAWT Design'' (August, 1994),
—— An unpublished report of project No. MNES/AE/9271

in Aerospace & Mechanical Engg. Department,
I I T Kanpur.

33. ''Design of 10kW VGVAWT —— Wind Turbine Statics''
and ''Wind Turbine Dynamics'',
—— Unpublished reports of VGVAWT design of project No.
MNES/AE/9271 by J. Singh (Project Research Associate
in Aerospace Engg. Department ,I I T Kanpur).

34. ''Design of a 10 kW Wind Turbine for Cyclone Prone Areas'',
—— by K. Ghosh et al (July,1995),
An unpublished paper (preprint submitted to Elsevier
Preprint).

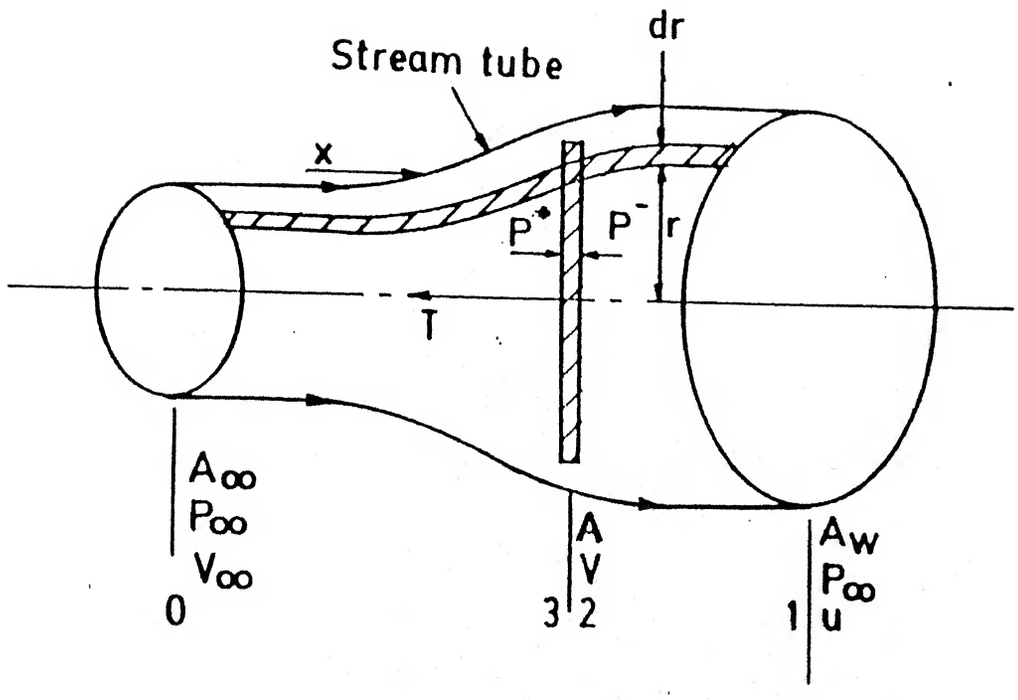

Fig. 2.1 Flow past a wind turbine

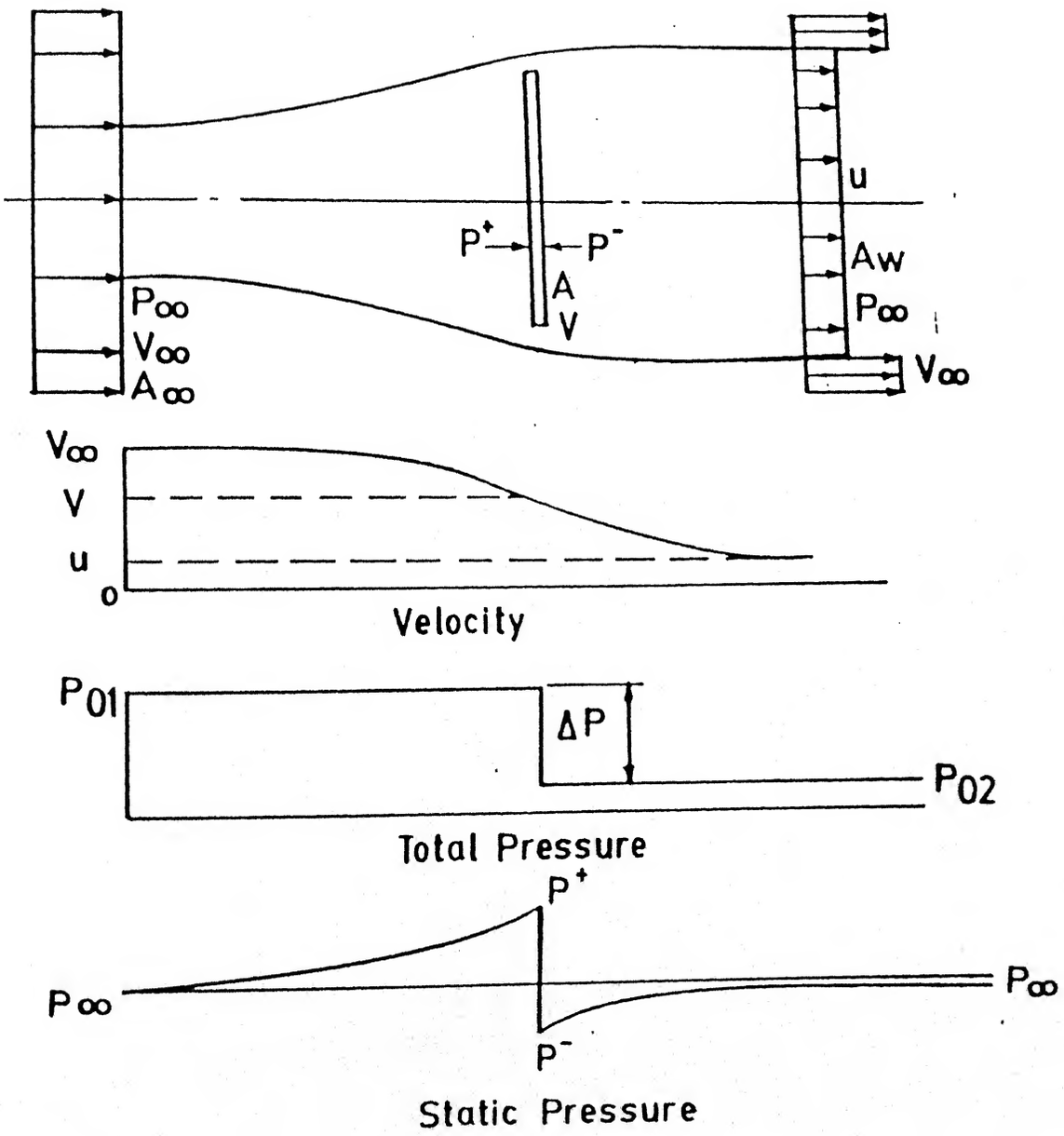

Fig. 2.2 Flow properties along a wind turbine

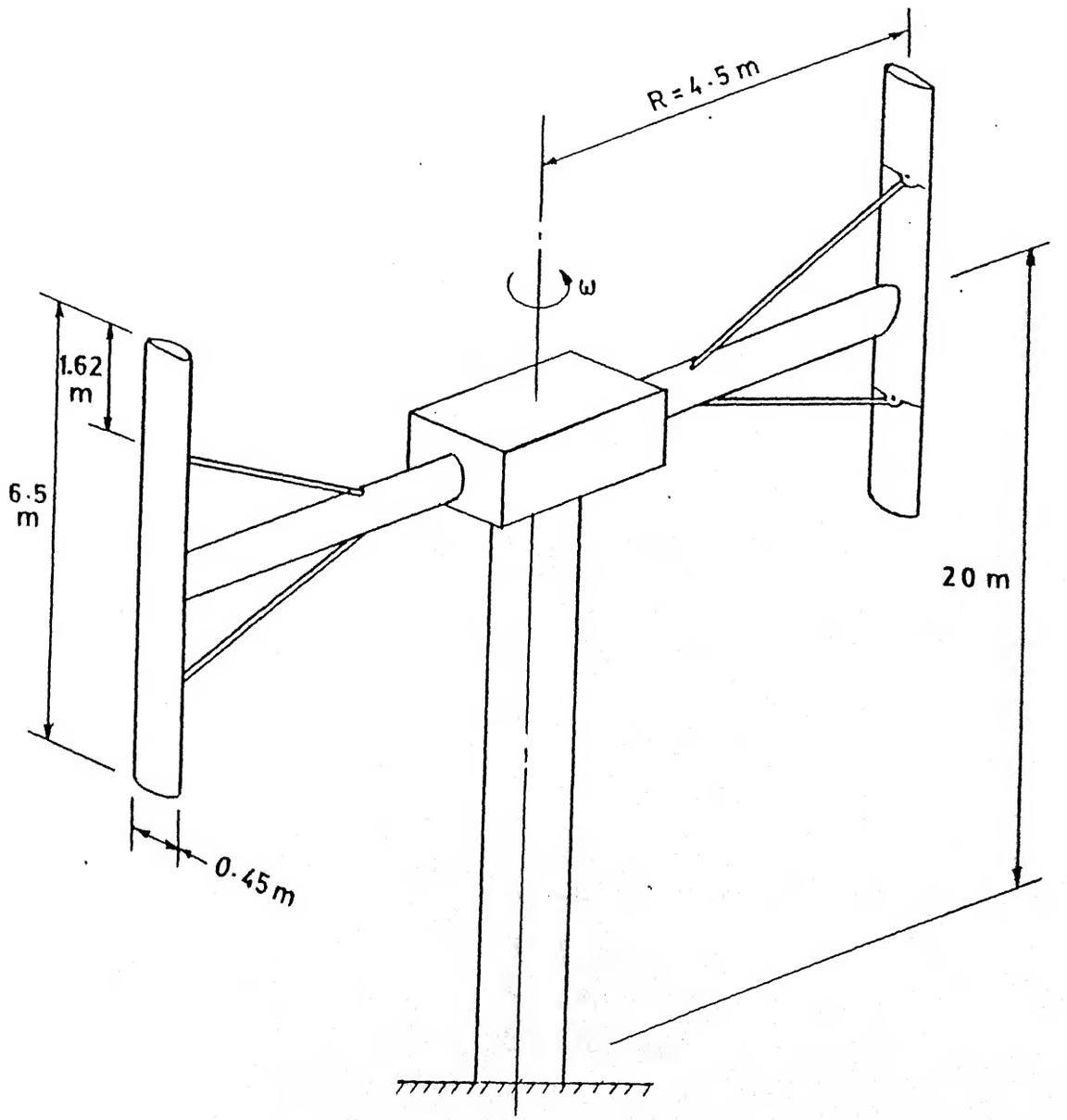

Fig. 3.1 General arrangement of a VGVAWT

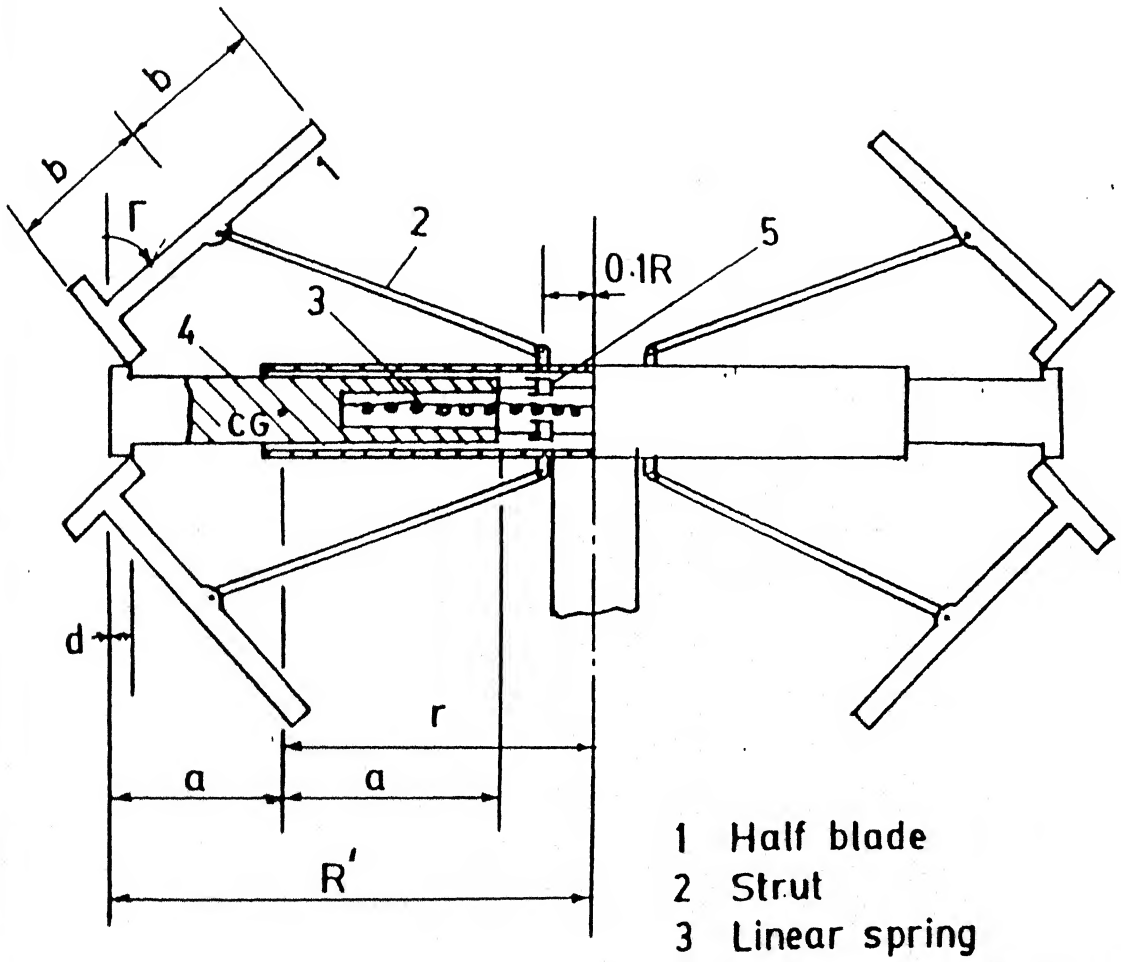

1 Half blade
2 Strut
3 Linear spring
4 Telescopic cross arm
5 Damper

Fig.3.2 Details of Rotor

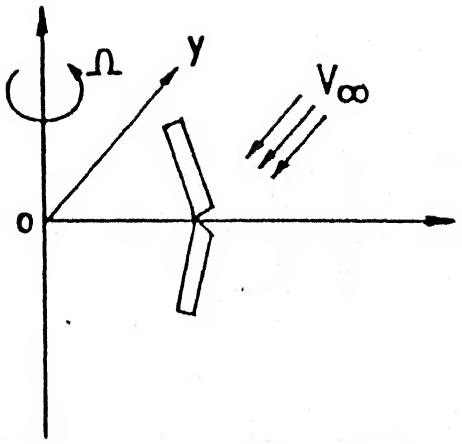

Fig. 4.1 Rotor geometry

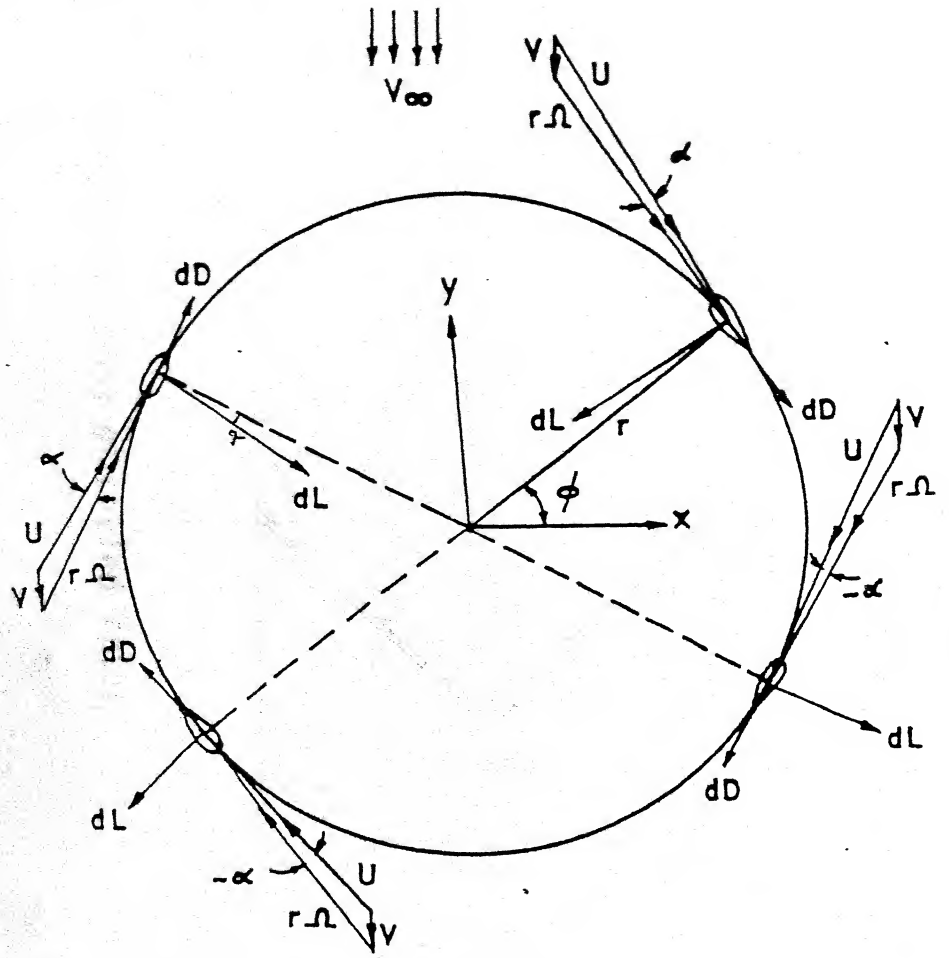

Fig. 4.2 Angle of attack variation with ϕ for $r\Omega > V$

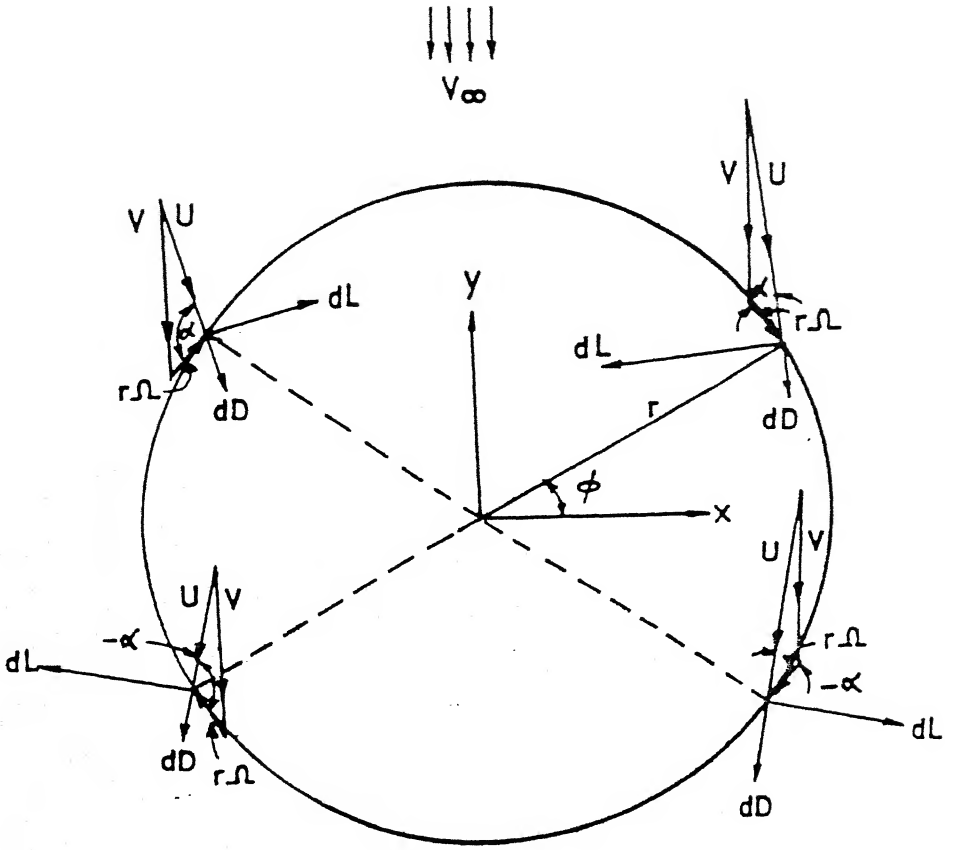

Fig. 4.3 Angle of attack variation with ϕ for $r\Omega < V$

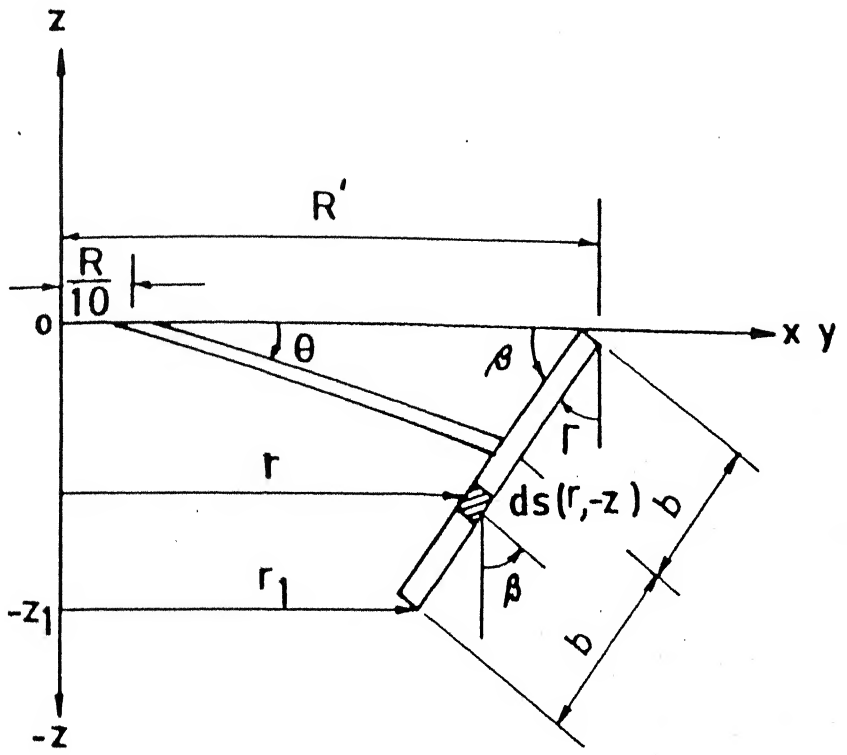

Fig. 4.4 Coordinates of blade element

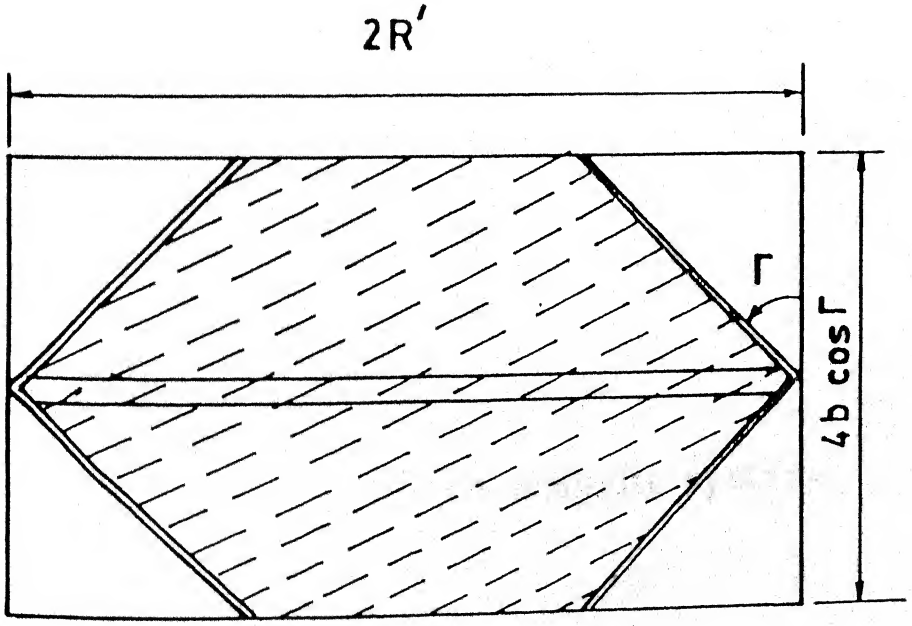

Fig. 4.5 Swept area of reefed rotor

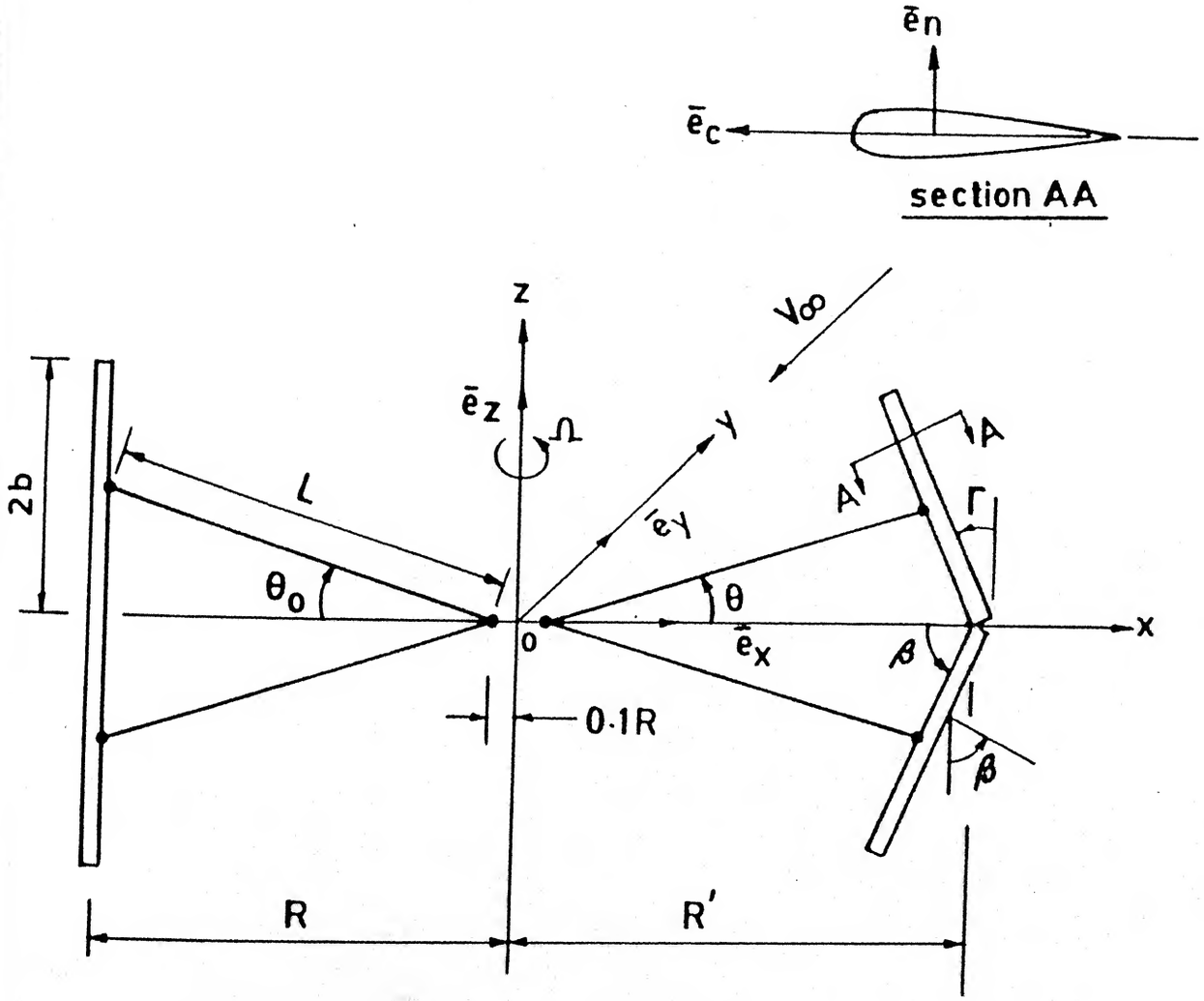

Fig. 4.6 The co-ordinate system

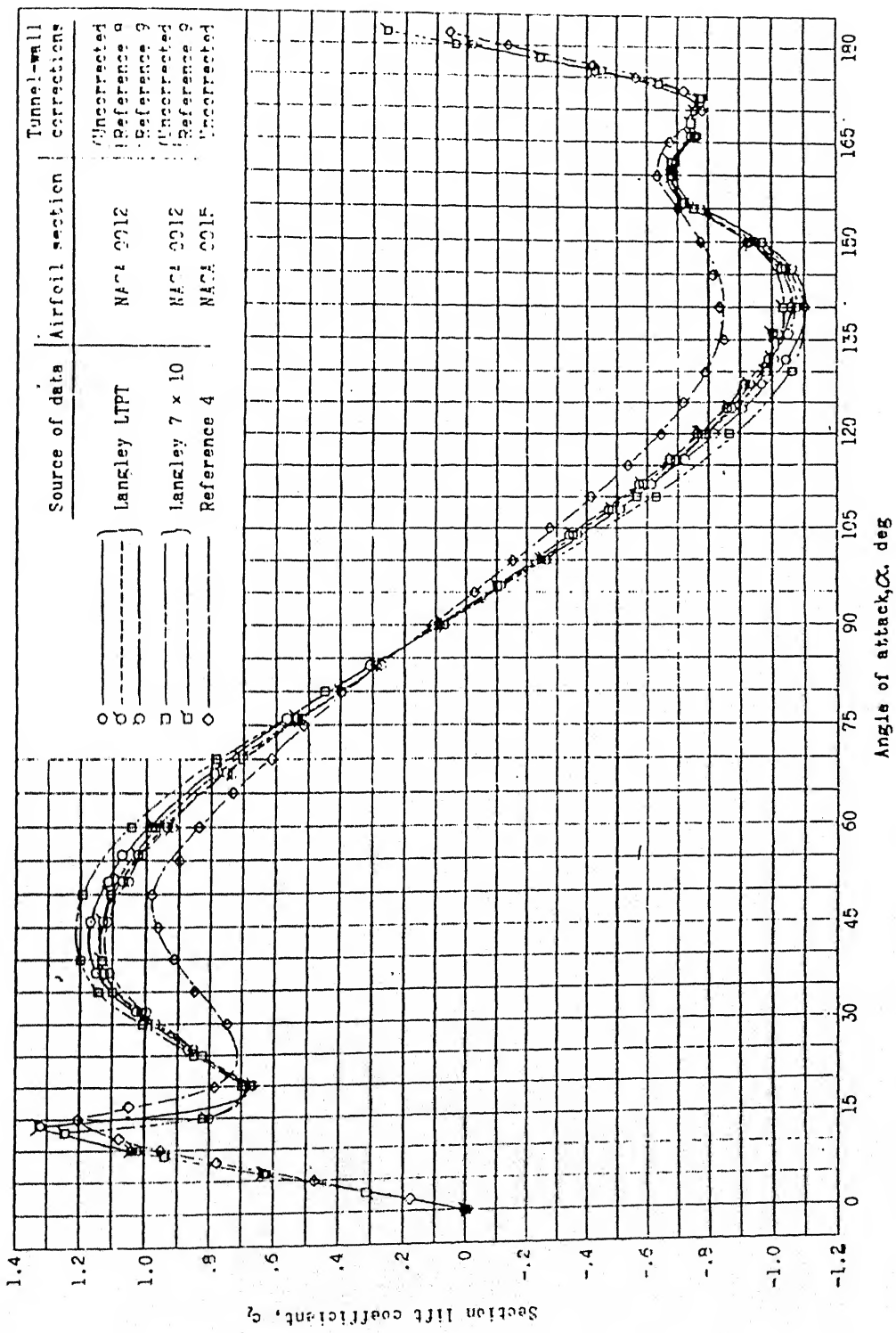

Fig(5.1a) Cl Vs α for NACA 0012 (Ref.5)

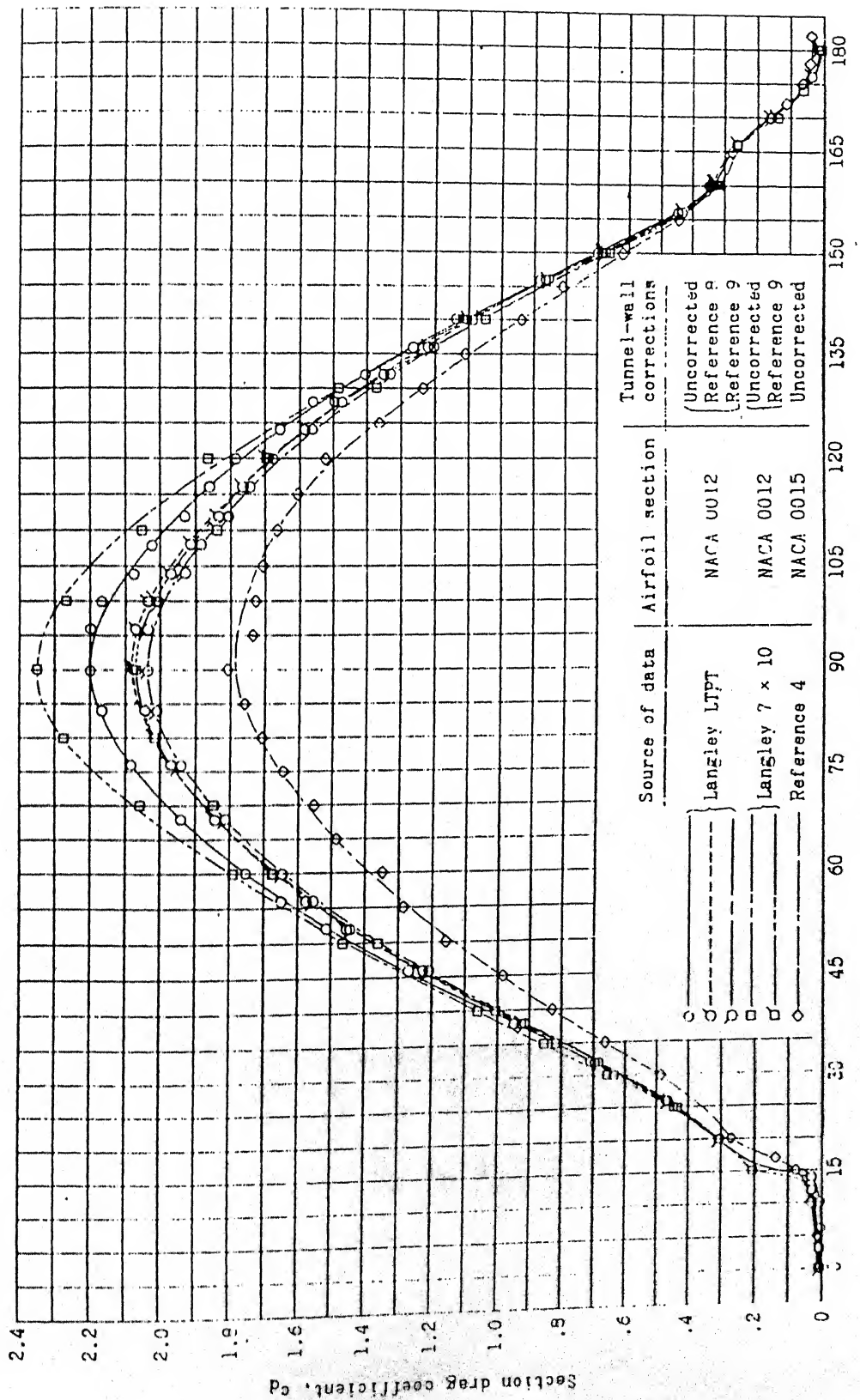

Fig(5.1b) Cd Vs α for NACA 0012 (Ref.5)

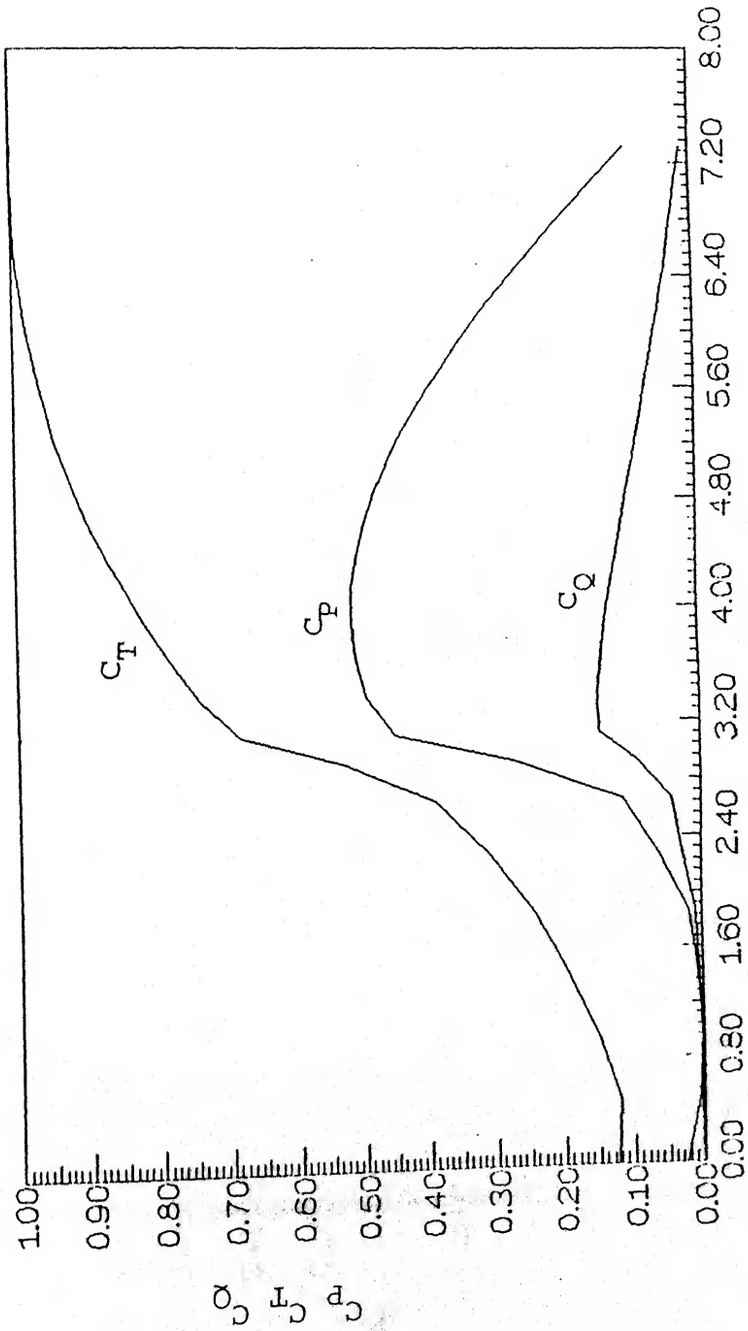

Fig.(5.2) C_P, C_T, C_Q versus tipspeed ratio
(for $\beta = 90°$)

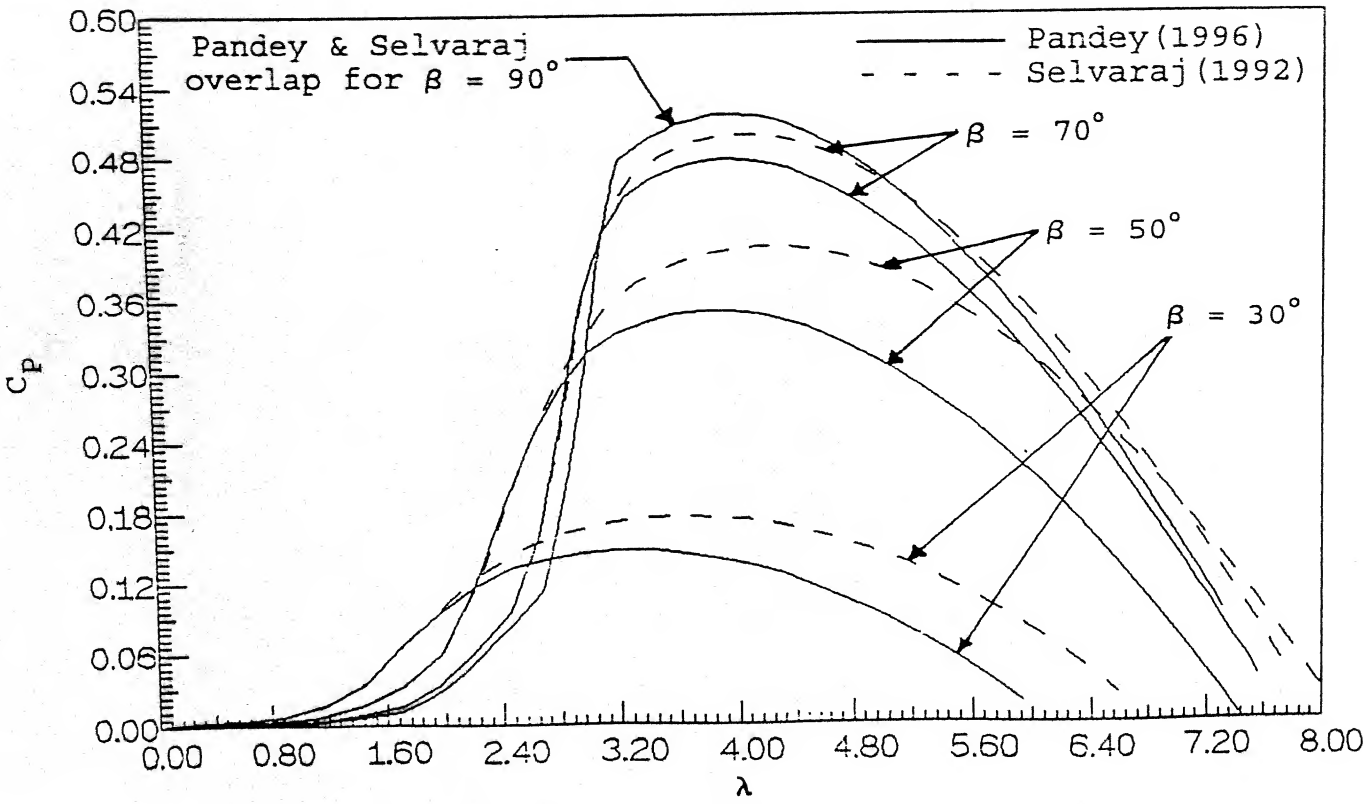

Fig.(5.3) Power coefficient versus tipspeed ratio for various arrowhead angles

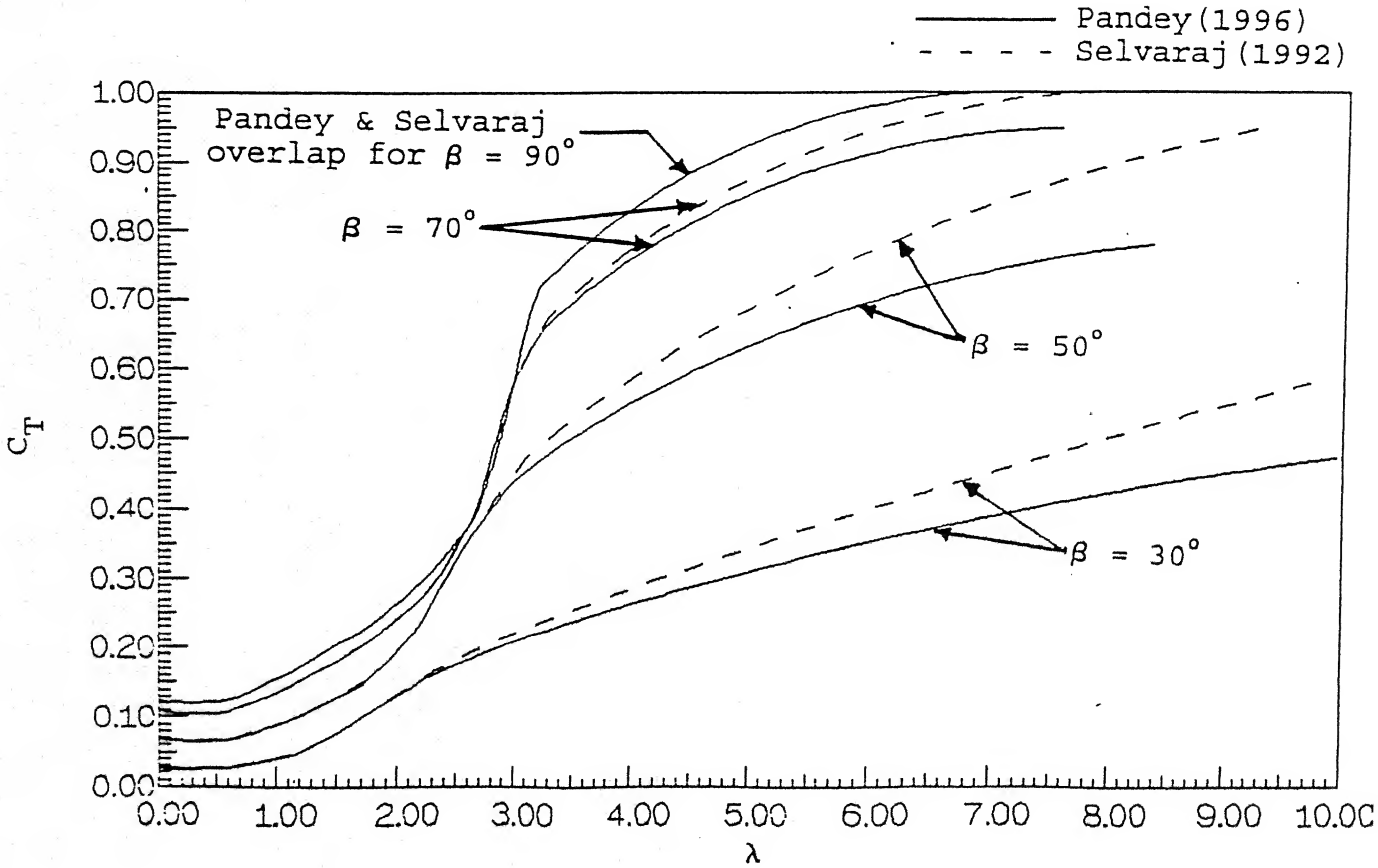

Fig.(5.4) Thrust coefficient versus tipspeed ratio for various arrowhead angles

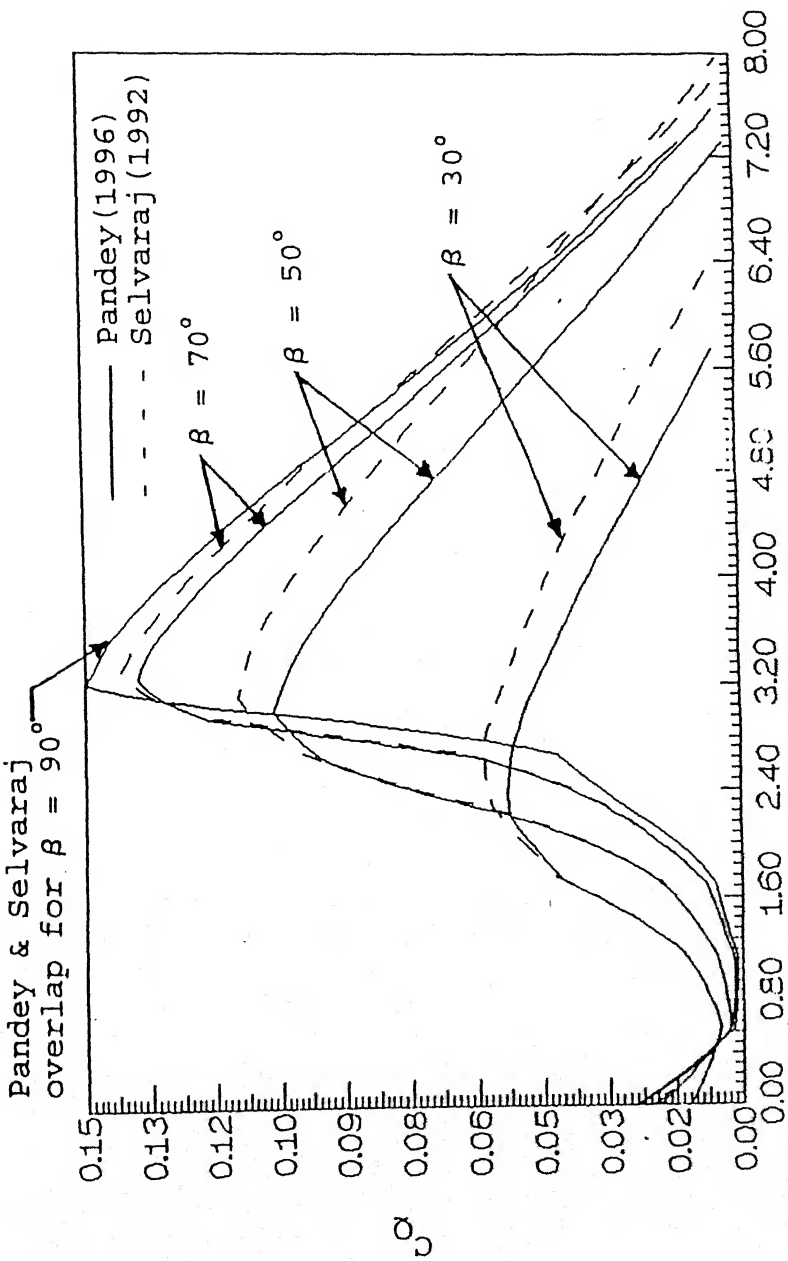

Fig.(5.5) Torque coefficient versus tipspeed ratio for various arrowhead angles

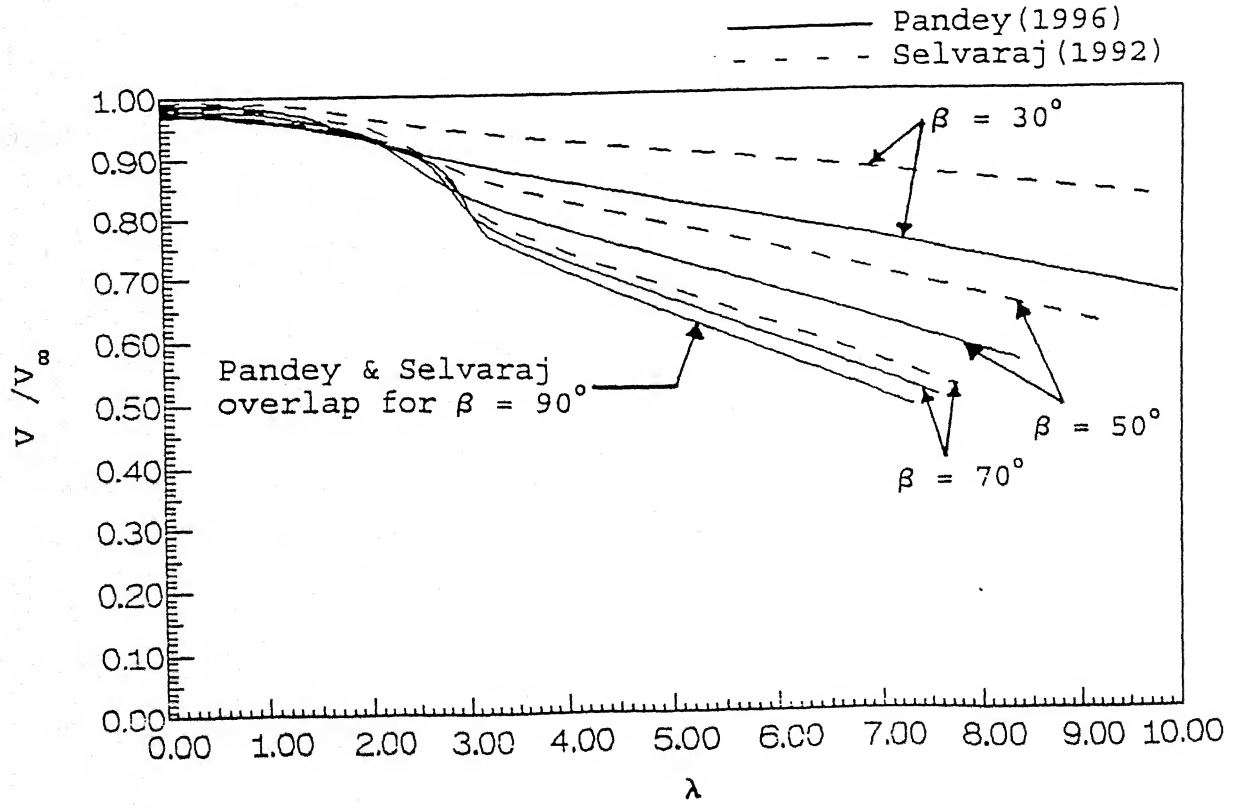

Fig.(5.6) Velocity ratio versus tipspeed ratio for various arrowhead angles

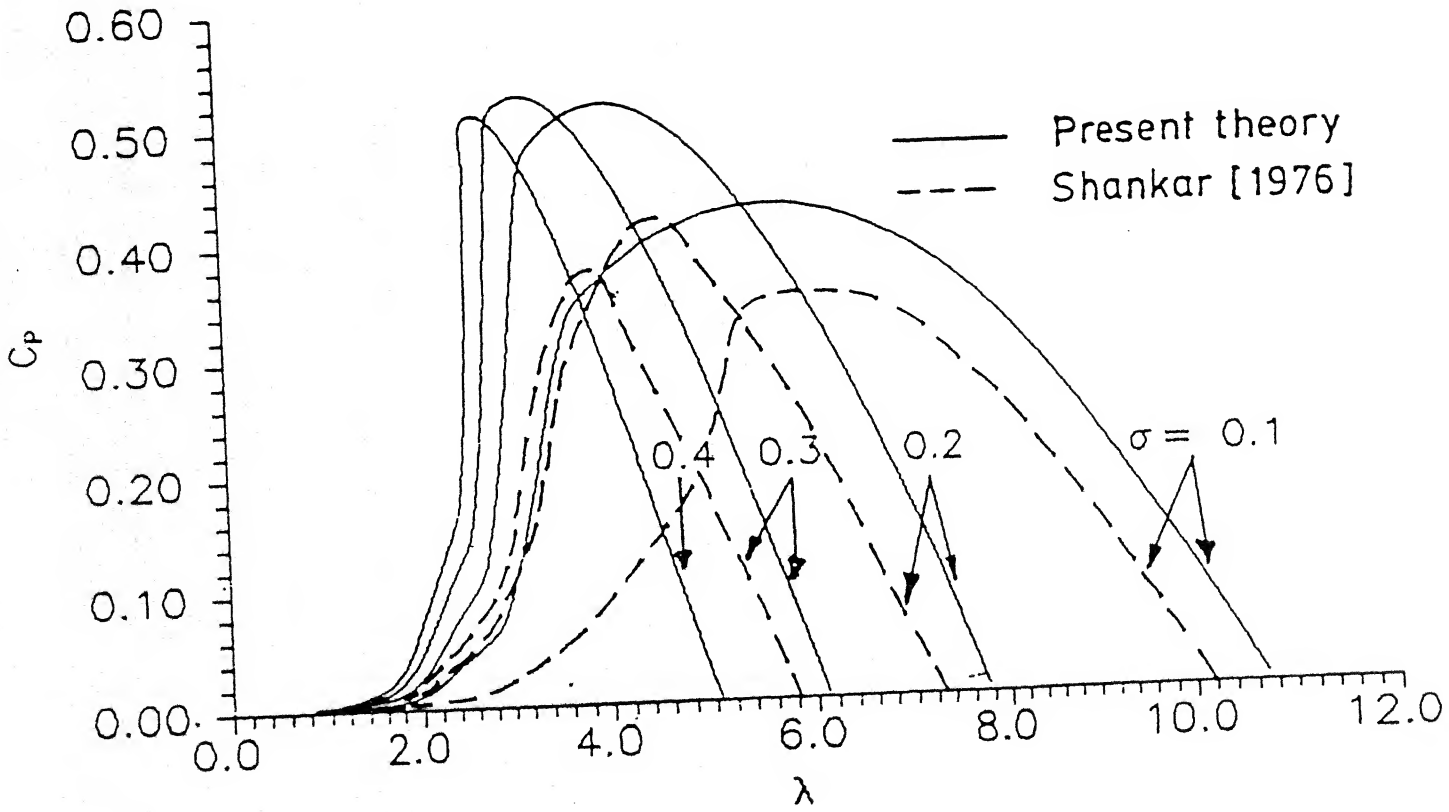

Fig. (5.7) Effect of solidity on power coefficient for $\beta = 90^0$

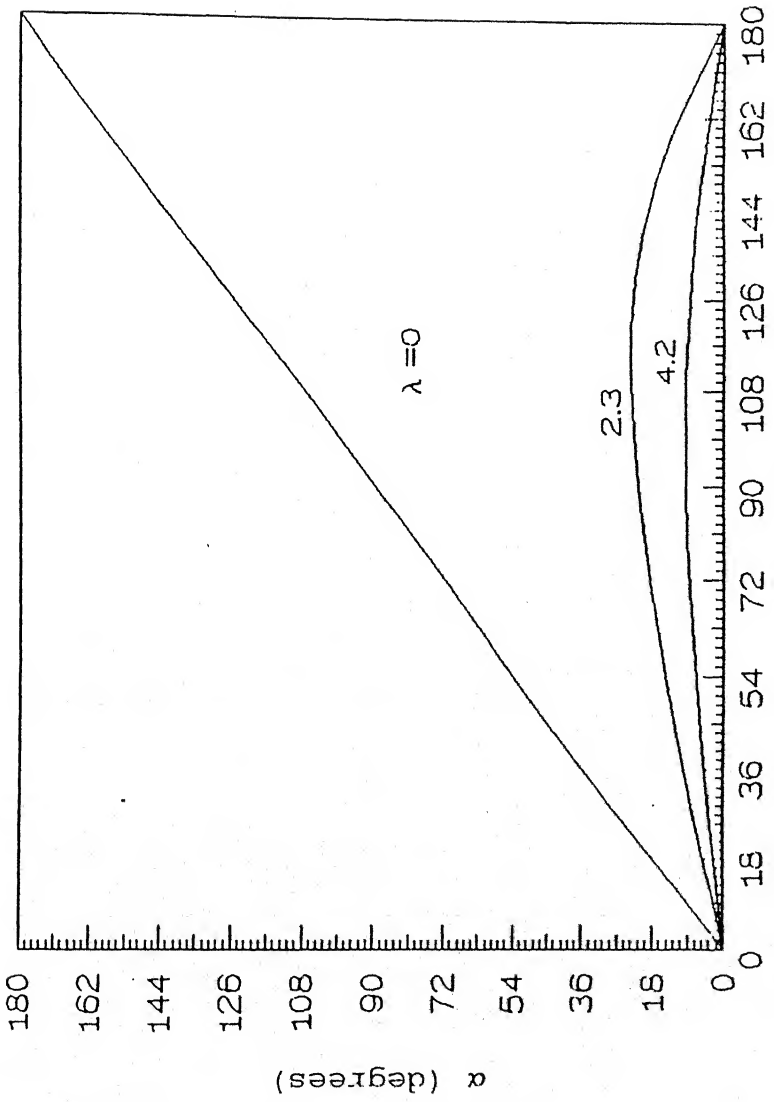

Fig.(5.8) Angle of attack versus Azimuthal angle for various tipspeed ratios ($\beta = 90^{\circ}$)

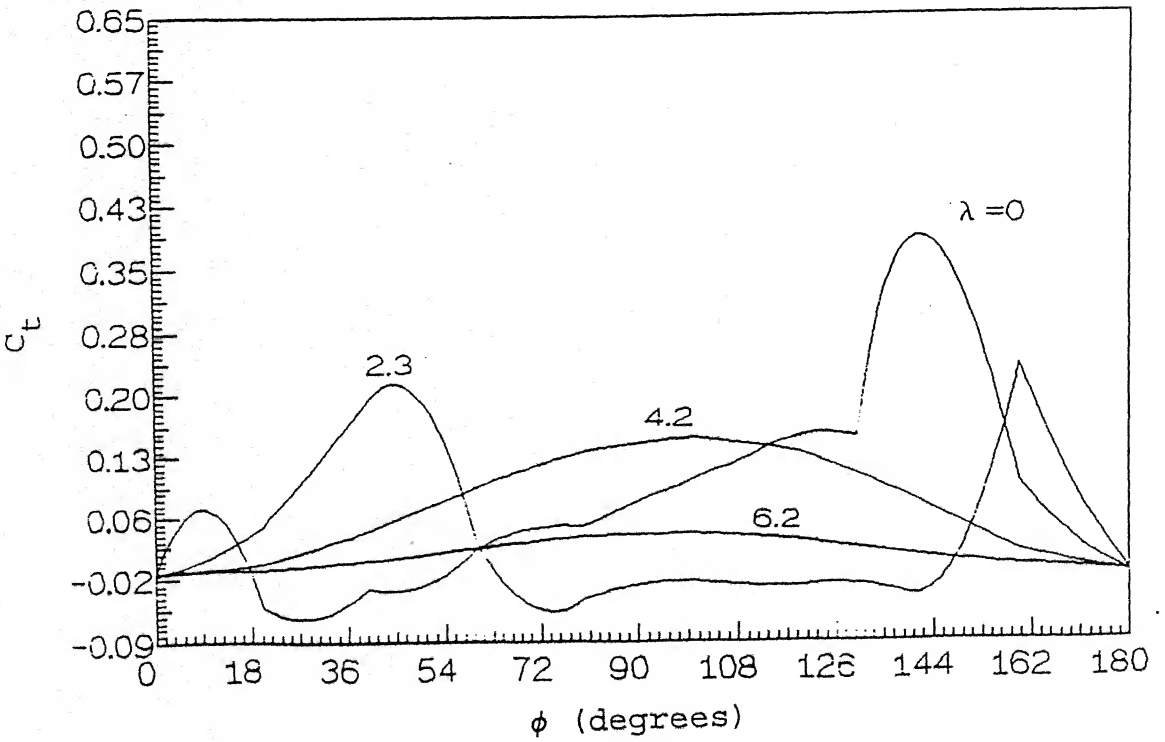

Fig.(5.9) Tangential force coefficient versus Azimuthal angle for various tipspeed ratios ($\beta = 90^{\circ}$)

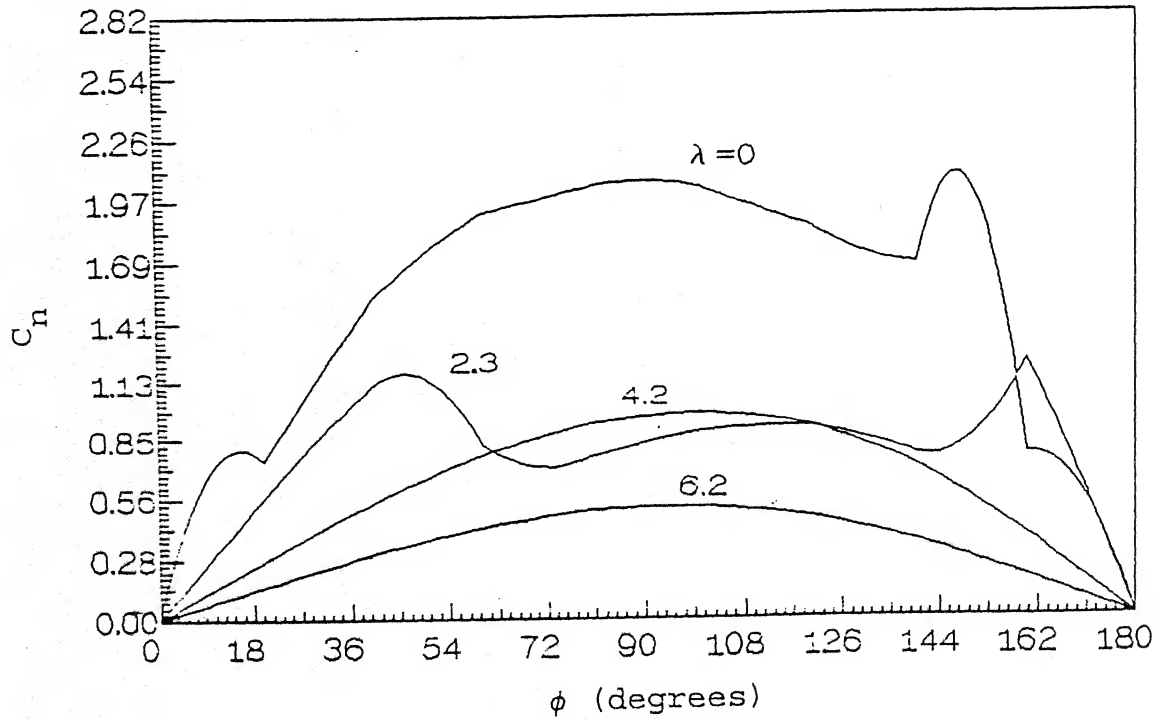

Fig.(5.10) Normal force coefficient versus Azimuthal angle for various tipspeed ratios ($\beta = 90°$)

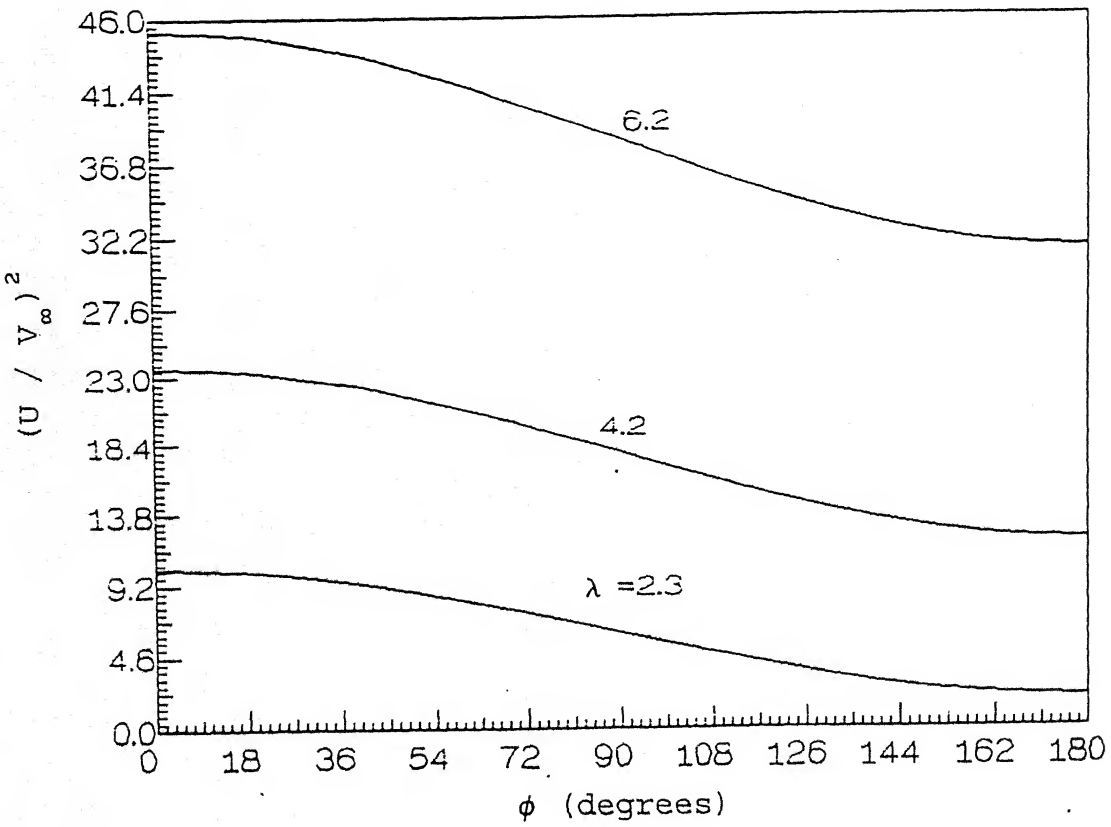

Fig.(5.11) $(U / V_\infty)^2$ versus Azimuthal angle for various tipspeed ratios ($\beta = 90^\circ$)

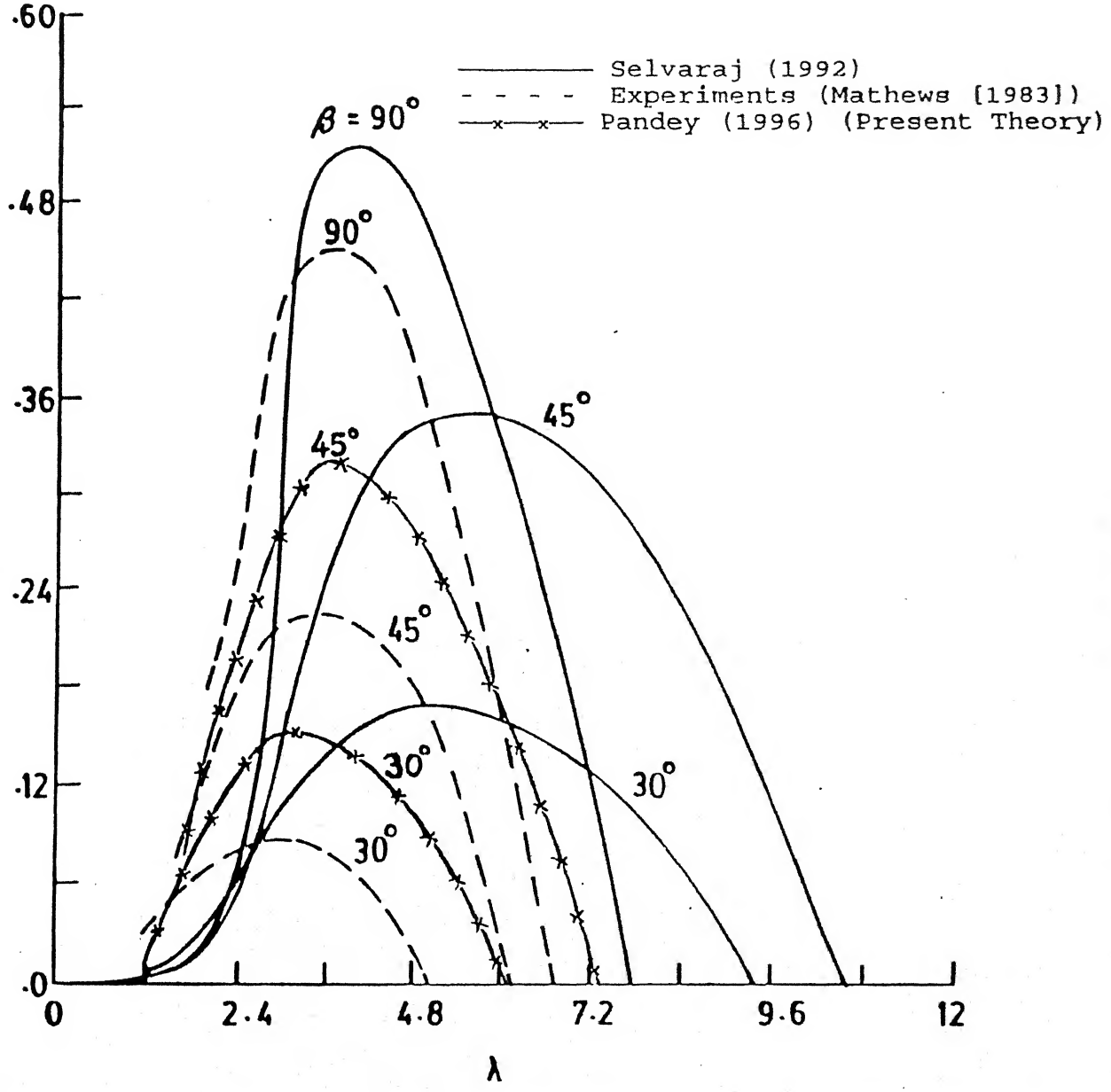

5.12 Comparison of power coefficient with experiments

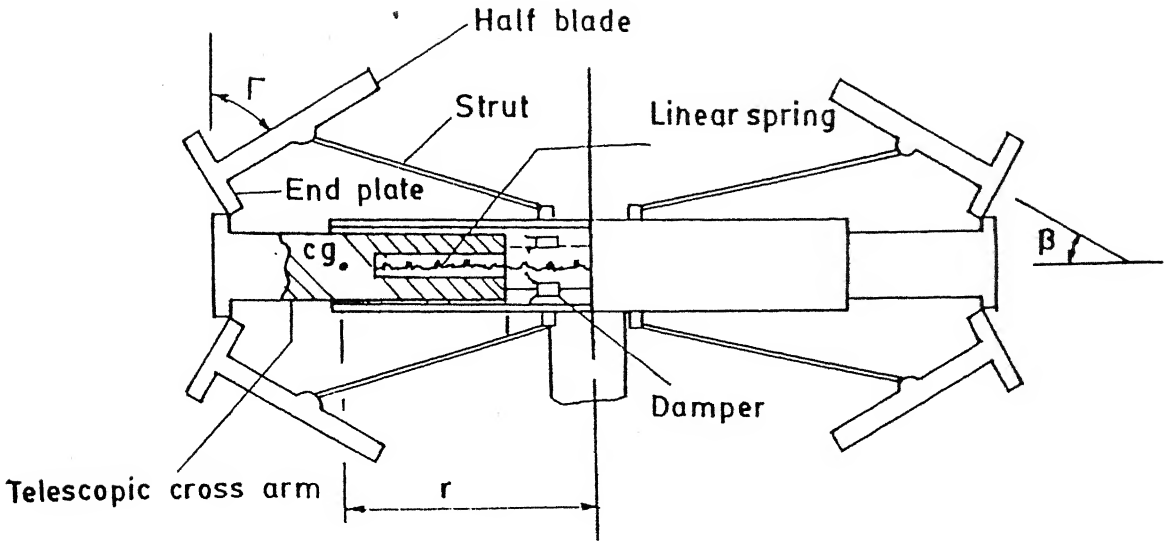

Fig. (6.1) Reef Control Mechanism

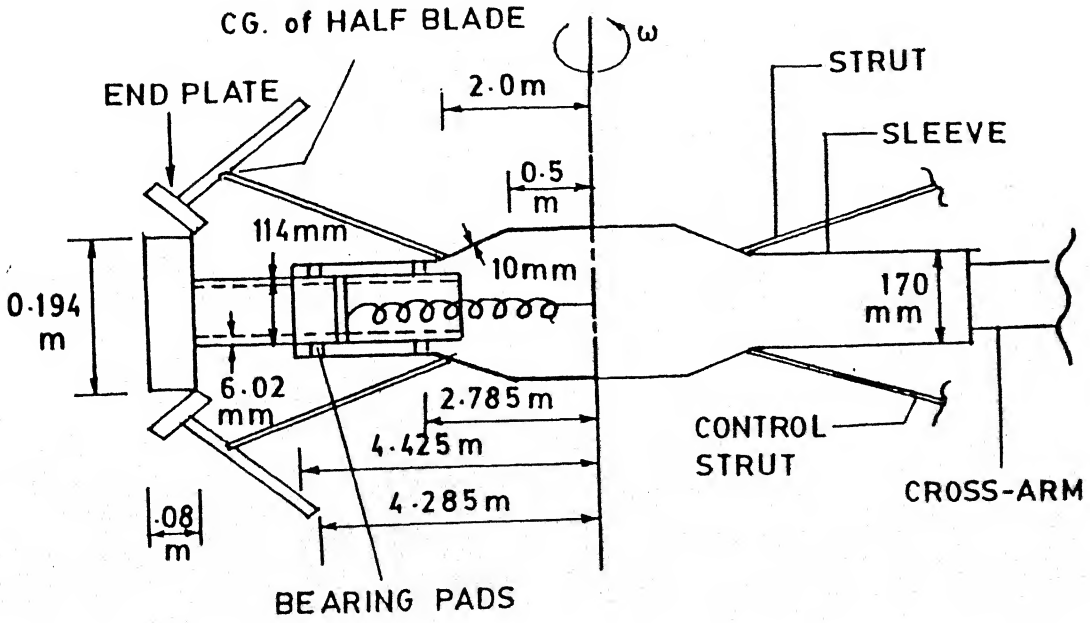

Fig. (6.2) Details of the Rotor : Front View
(Z - Link omitted for clarity)

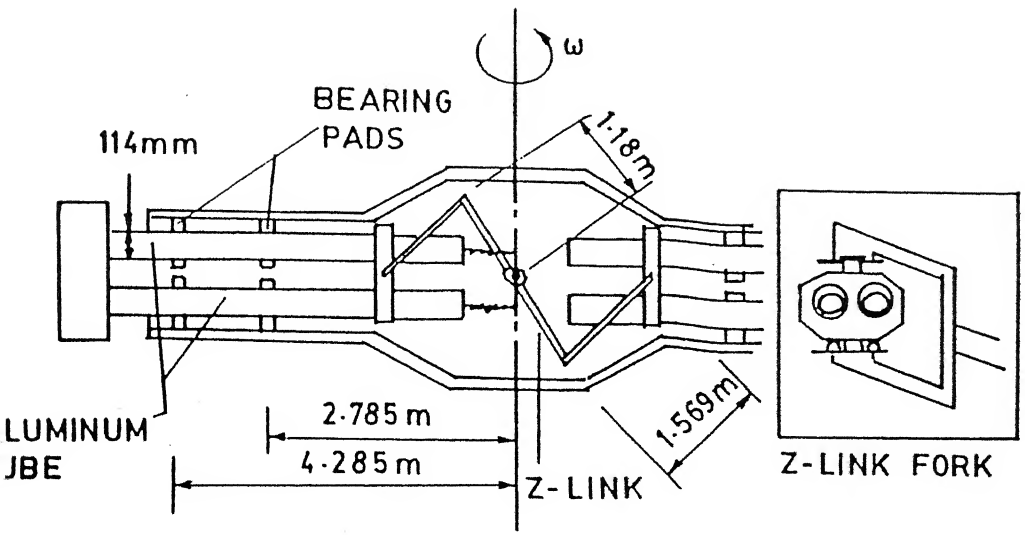

Fig. (6.3) Z - Link Configuration connecting opposed Cross-arms : Top View

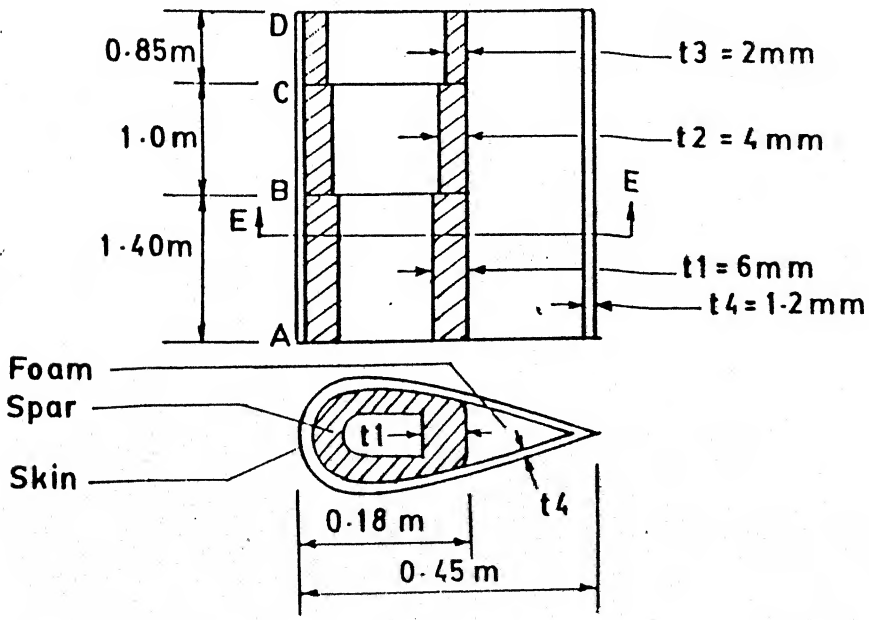

Fig. (6.4) Structural Details of the FRP Blade

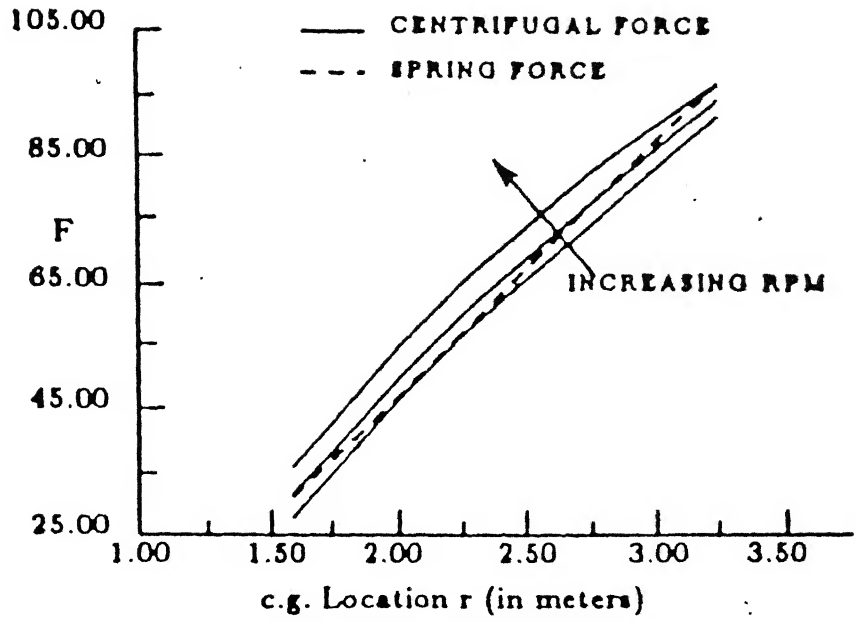

Fig. (6.5) Centrifugal Force Curves
(F = Force per unit mass of Half Blade (kgf/kg))

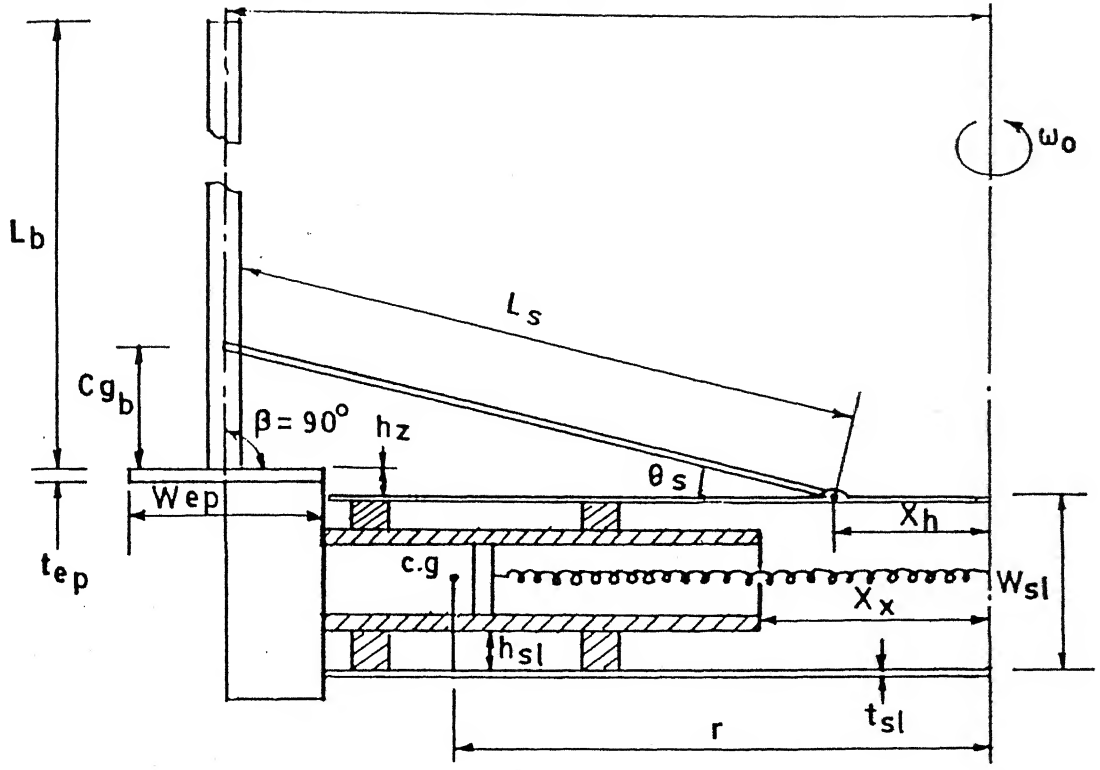

Fig. (6.6) Wind Turbine Assembly (Unreefed)

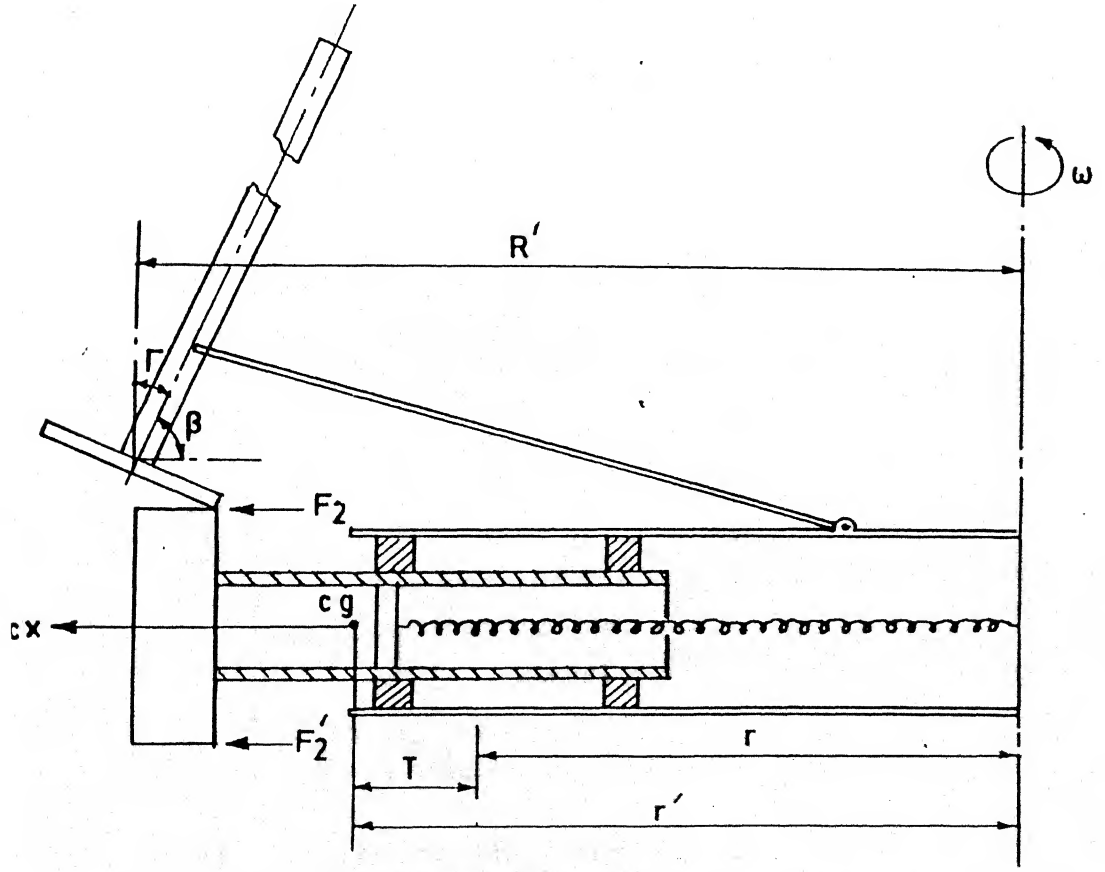

Fig. (6.7) Wind Turbine Assembly (Reefed)

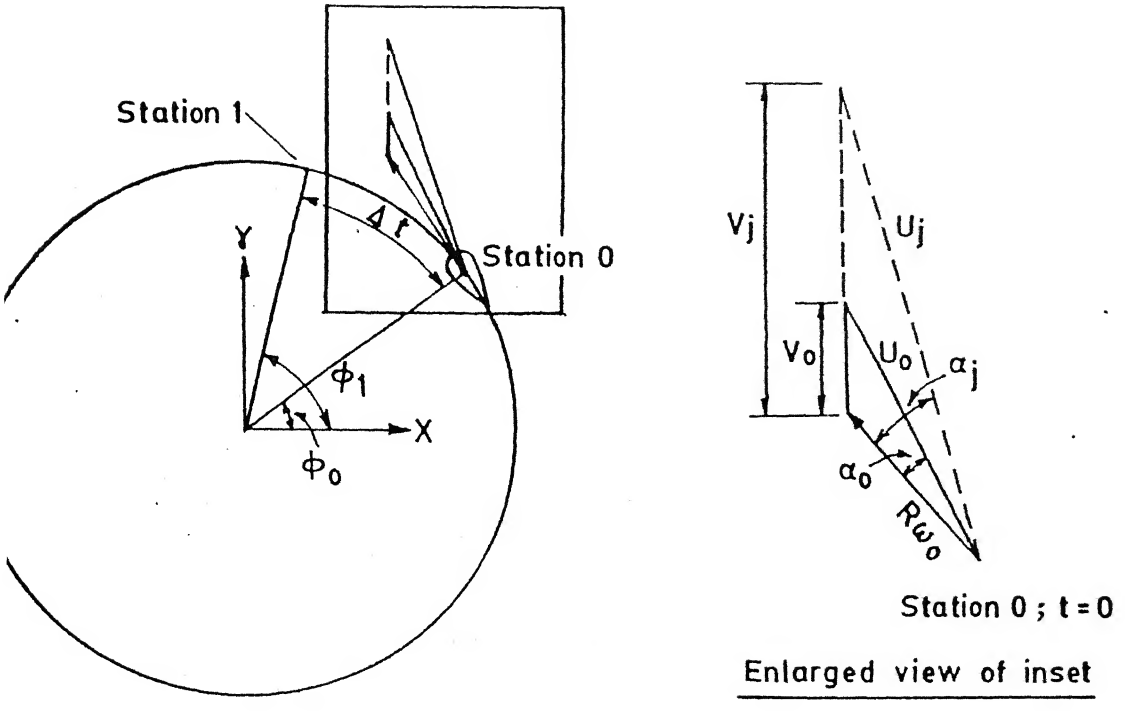

Fig. (6.8) Velocities at the Wind Turbine Blade at station O

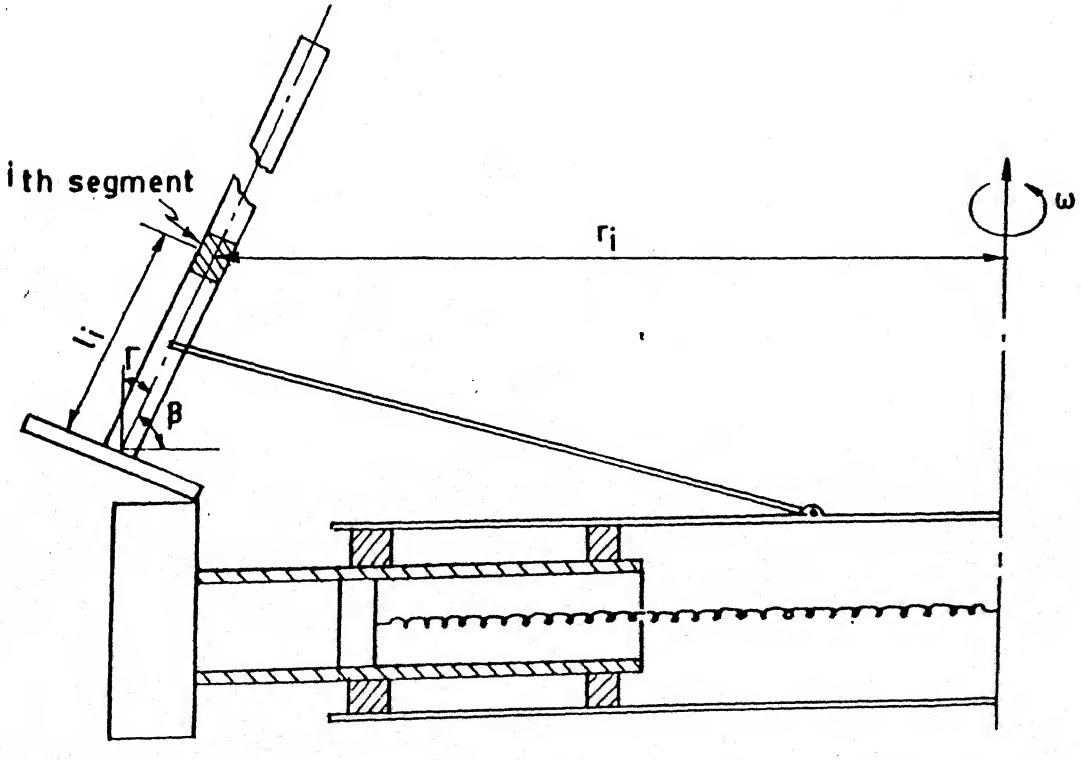

Fig. (6.9) A View of the Wind Turbine Half Blade (reefed) discretized into N segments

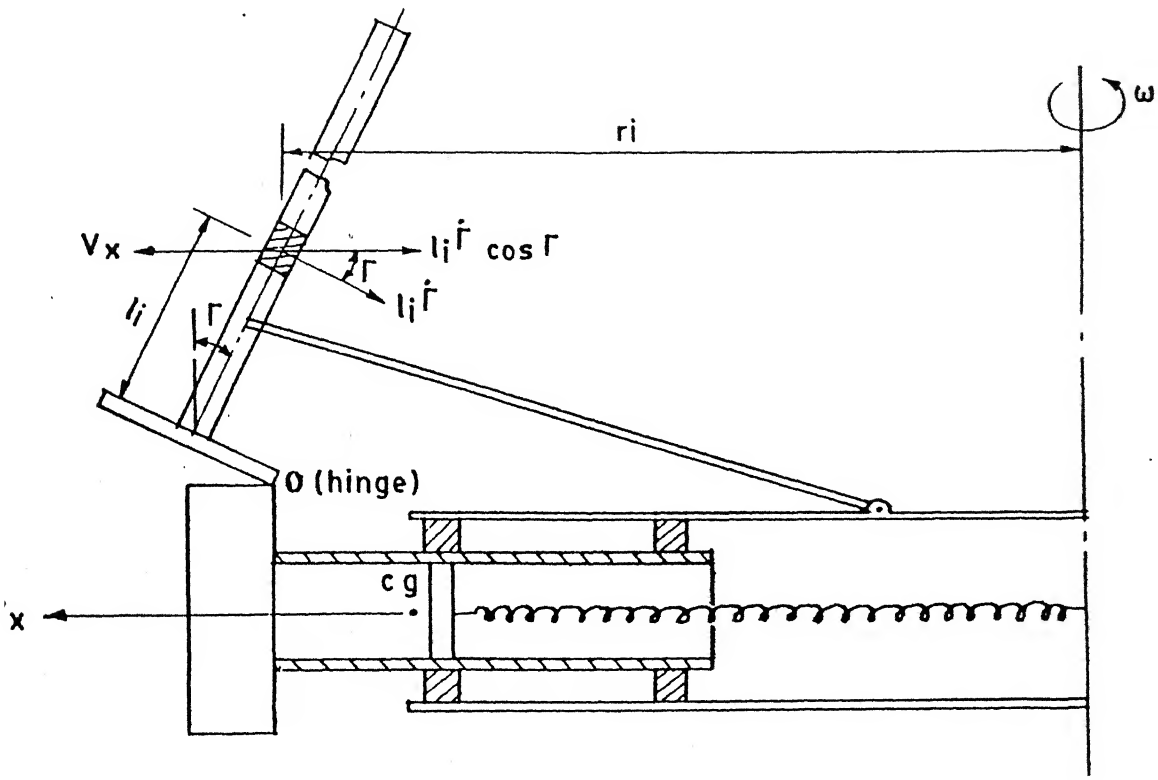

Fig. (6.10) Linear radial velocity of the i^{th} segment of the Half Blade

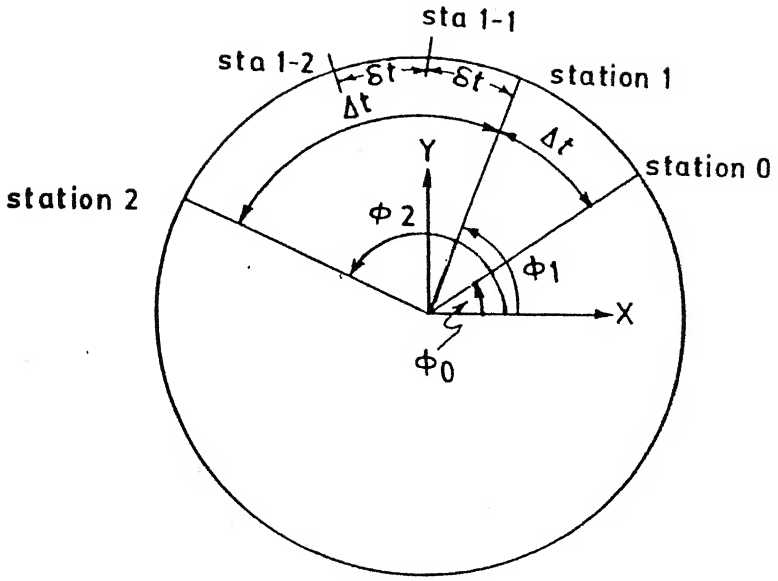

Fig. (6.11)

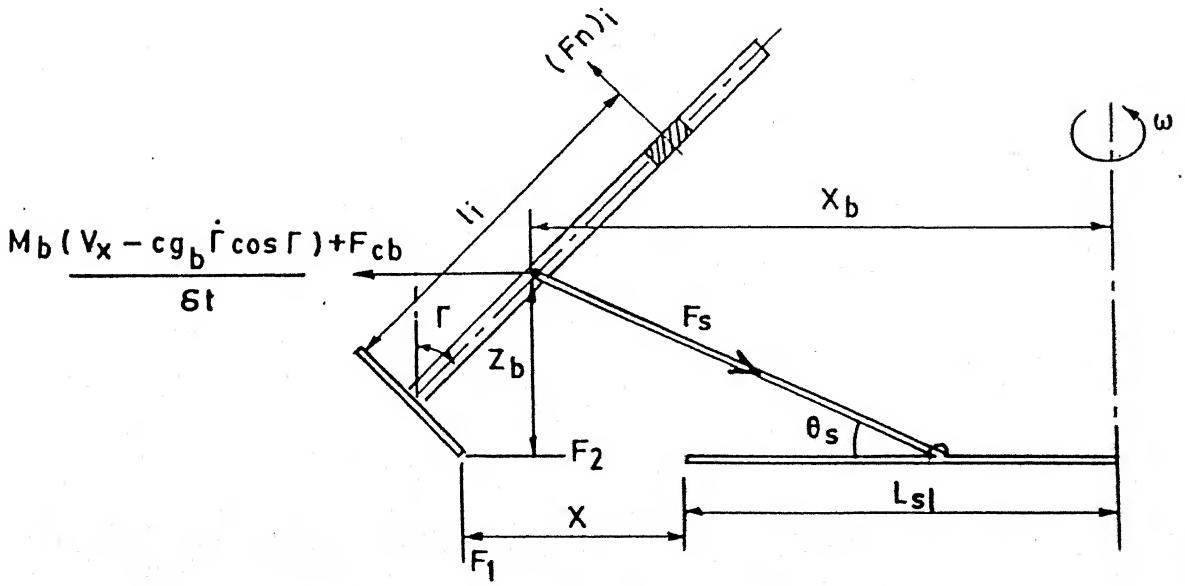

Fig. (6.12) Perturbation forces on the Wind Turbine Half Blade in reef

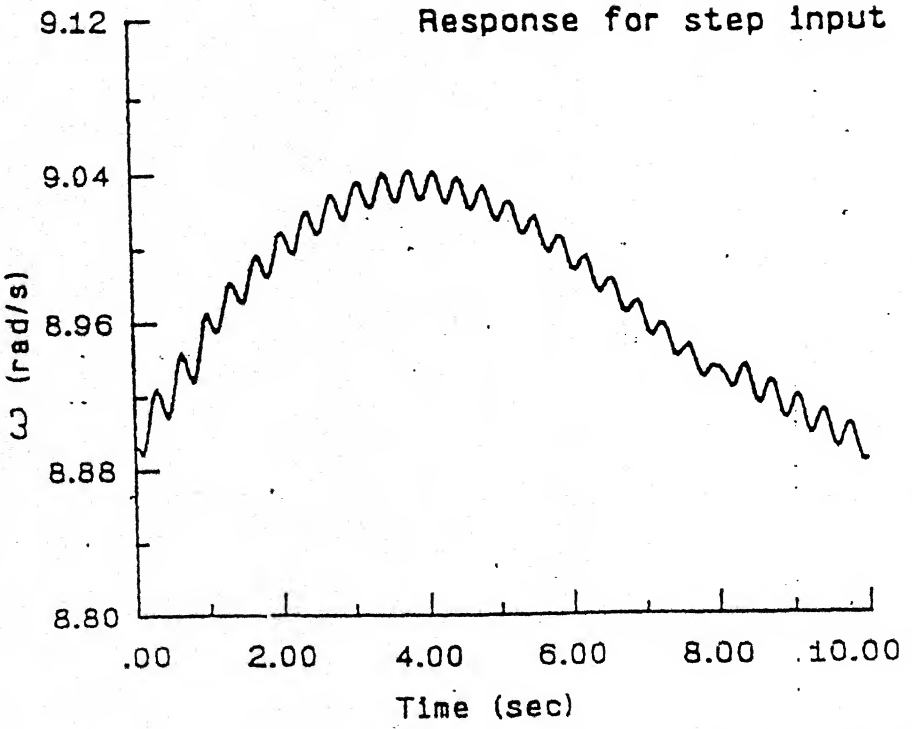

Fig. (6.13 a) Time history of angular velocity (ω)

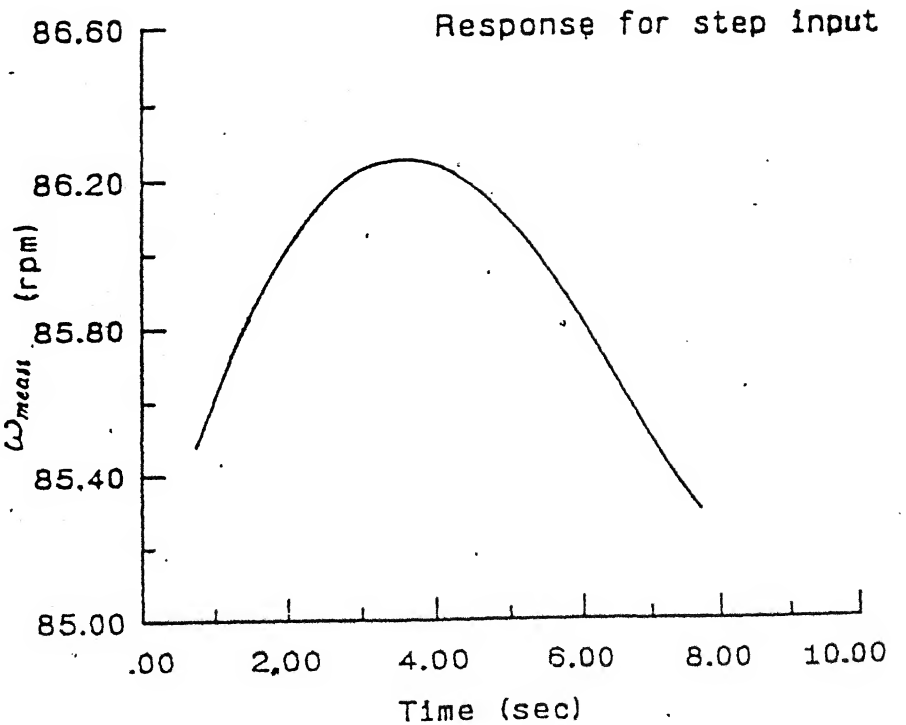

Fig. (6.13 b) Time history of mean angular velocity (ω_{mean})

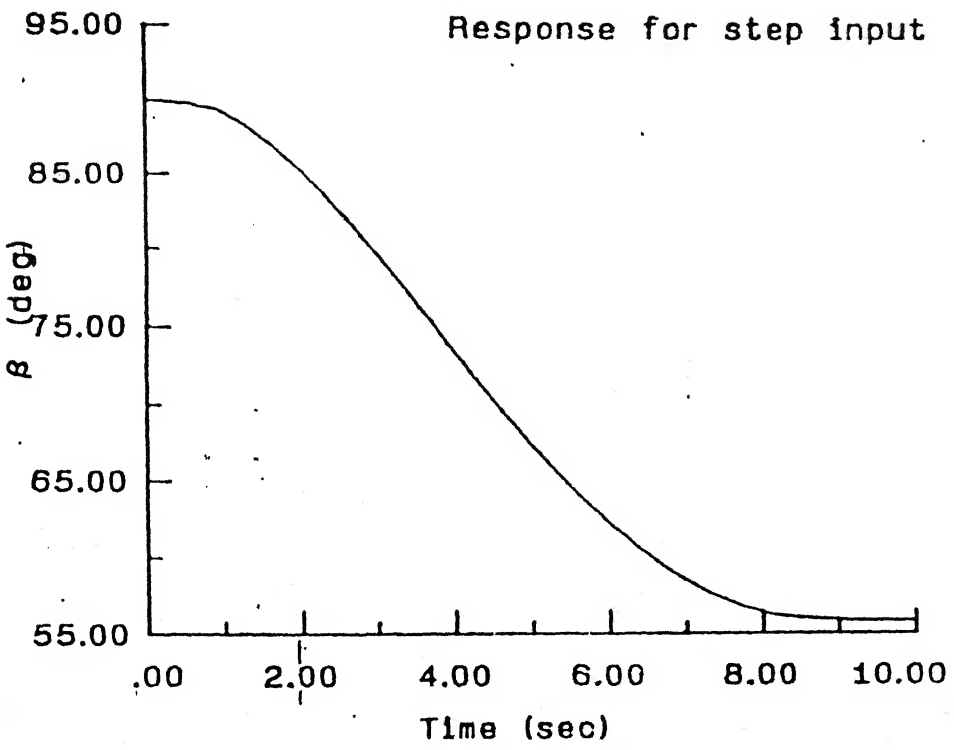

Fig. (6.14) Time history of arrowhead angle (β)

APPENDIX 1 : *Elongation of Rotating Spring*

Total number of coils = 220

Free length = 3000 mm

Therefore, each coil length = 3000 / 220 = 13.6 mm

Mass of the spring = 58 Kg

Mass M of each coil = 58 / 220 = 0.26 Kg

Spring stifness = 0.4 Kgf/mm

Stiffness of each coil = $0.4 \times 9.81 \times 10^3 \times 220 = 863.28 \times 10^3$ N/m

Centrifugal force in the 1st coil = $Mr\omega^2 = 0.26 \times r \times \omega^2$ N

where $r = 13.6 \times 10^{-3}$ m and $\omega = 8.9$ rad/s

Elongation Δr of the 1st coil = $\frac{0.26 \times r \times \omega^2}{863.28 \times 10^3}$

$$\Delta r = 3.01176 \times 10^{-7} \, r\omega^2 \text{ meters}$$

Centrifugal force due to the 2nd coil = $M(2r)\omega^2$ Newtons

Therefore, elongation of the 2nd coil = $2\Delta r$ and net elongation upto the 2nd coil = $2\Delta r + \Delta r$

Similarly, net elongation upto the 3rd coil = $3\Delta r + 2\Delta r + \Delta r$

Therefore, net elongation upto the 220th coil = $220\Delta r + \ldots + 3\Delta r + 2\Delta r + \Delta r$

Hence, net elongation in the spring due to the centrifugal force generated by its own mass =

$$[\frac{220 \times 221}{2}] \Delta r = 24310 \, \Delta r$$

$$= 7.88 \times 10^{-3} \text{ meters}$$

$$\simeq 8.0 \text{ mm}$$

When fully reefed, the spring stretches approximately to twice its length. The value of r in that case will approximately be equal to 27 mm and the elongation in the spring (rpm remains constant) due to its own mass goes upto 16 mm.

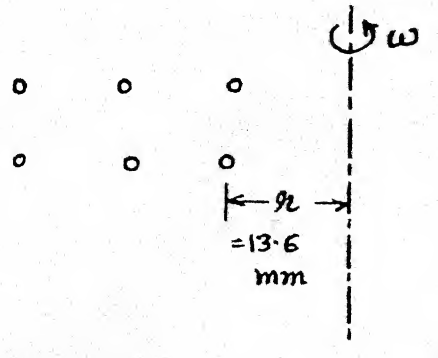

A 121747

Date Slip

This book is to be returned on the date last stamped.